eprints@whiterose.ac.uk
https://eprints.whiterose.ac.uk/

arXiv:0910.0174v3 [hep-ph] 18 Jan 2010

Supersymmetric particle mass measurement with the boost-corrected contransverse mass

Giacomo Polesello,

INFN, Sezione di Pavia, Via Bassi 6, 27100 Pavia, Italy
E-mail: `giacomo.polesello@cern.ch`

Daniel R. Tovey,

Department of Physics and Astronomy,
University of Sheffield, Hounsfield Road, Sheffield S3 7RH, UK
E-mail: `daniel.tovey@cern.ch`

ABSTRACT: A modification to the contransverse mass (M_{CT}) technique for measuring the masses of pair-produced semi-invisibly decaying heavy particles is proposed in which M_{CT} is corrected for non-zero boosts of the centre-of-momentum (CoM) frame of the heavy states in the laboratory transverse plane. Lack of knowledge of the mass of the CoM frame prevents exact correction for this boost, however it is shown that a conservative correction can nevertheless be derived which always generates an M_{CT} value which is less than or equal to the true value of M_{CT} in the CoM frame. The new technique is demonstrated with case studies of mass measurement with fully leptonic $t\bar{t}$ events and with SUSY events possessing a similar final state.

Contents

1. Introduction

Techniques for measuring the masses of pair-produced particles decaying semi-invisibly through short decay chains at hadron colliders have attracted considerable interest. The principle motivation for the development of such techniques is the measurement of the masses of supersymmetric particles ('sparticles') at the Large Hadron Collider [1, 2, 3, 4, 5, 6, 7, 8, 9, 10, 11, 12, 13, 14, 15, 16], however they may be applied more widely to measure the mass of the top quark at the Tevatron [17] or LHC [18], or to identify fully leptonic WW events [19].

Recently [9] a straightforward new variable, the 'contransverse mass' (M_{CT}), was proposed which enables the measurement of a simple analytical combination of the masses of the pair-produced heavy states δ_i ($i = 1, 2$) and their invisible decay products α_i. The contransverse mass is defined by

$$M_{CT}^2(v_1, v_2) \equiv [E_T(v_1) + E_T(v_2)]^2 - [\mathbf{p_T}(v_1) - \mathbf{p_T}(v_2)]^2$$

$$= m^2(v_1) + m^2(v_2) + 2[E_T(v_1)E_T(v_2) + \mathbf{p_T}(v_1) \cdot \mathbf{p_T}(v_2)], \qquad (1.1)$$

where v_i are the visible products of each decay chain, $\mathbf{p_T}(v_i)$ is the tranverse momentum vector of v_i and

$$E_T(v_i) \equiv \sqrt{p_T^2(v_i) + m^2(v_i)}. \qquad (1.2)$$

It can be shown [9] that M_{CT} is in general bounded from above by a quantity dependent upon the masses $m(\delta)$ and $m(\alpha)$. If $m(v_1) = m(v_2) \equiv m(v)$ then the distribution of event M_{CT} values possesses an end-point at:

$$M_{CT}^{\max}[m^2(v)] = \frac{m^2(v)}{m(\delta)} + \frac{m^2(\delta) - m^2(\alpha)}{m(\delta)}. \qquad (1.3)$$

Consequently a measurement of the gradient and intercept of the linear function describing the dependence of $M_{CT}^{\max}$ on $m^2(v)$ allows both $m(\delta)$ and $m(\alpha)$ to be measured independently.

Despite the simplicity and ease-of-use of the contransverse mass technique, it suffers from two principle draw-backs [9]. The first is that M_{CT} is not invariant under Lorentz boosts of the $\delta_1\delta_2$ centre-of-momentum (CoM) frame in the laboratory transverse plane. Consequently if the $\delta_1\delta_2$ system recoils in the transverse plane against upstream object(s) such as ISR jets then the value of M_{CT} calculated in the laboratory frame is not in general equal to that calculated in the $\delta_1\delta_2$ CoM frame. M_{CT} values can be generated which are greater than $M_{CT}^{\max}$ and as a result the M_{CT} end-point can be smeared (see e.g. Figure 2 in Ref. [9]). The second draw-back is apparent when attempting to measure $m(\delta)$ and $m(\alpha)$ independently in events with non-zero visible masses $m(v_i)$ using Eqn. (1.3). The requirement $m(v_1) = m(v_2)$ can significantly reduce the available event statistics and require the accumulation of very large integrated luminosity, even for channels with relatively large $\sigma.BR$. This problem is illustrated clearly in Figure 3 in Ref. [9]. This paper will seek to address these two problems and demonstrate the utility of the M_{CT} technique through two case-studies. In the process we shall identify a further problem with using Eqn. (1.3) to measure masses independently, but develop an alternative strategy for two-step sequential two-body decay chains combining M_{CT} end-point measurements with conventional invariant mass end-point constraints. We shall also investigate the use of the transverse boost dependence of $M_{CT}^{\max}$ to measure masses independently, but find that this technique suffers from similar problems.

The structure of the paper is as follows. Section 2 will study the transformation properties of M_{CT} under contra-linear and co-linear Lorentz boosts of δ_i, leading to the development of a procedure for correcting M_{CT} for co-linear boosts. Section 3 will discuss the shape of the resulting M_{CT} distributions. Section 4 will propose a new method for maximising the available event statistics when measuring $m(\delta)$ and $m(\alpha)$ independently with Eqn. (1.3) by removing the $m(v_1) = m(v_2)$ requirement. This section will also develop a technique through which $m(\delta)$ and $m(\alpha)$ can in principle be measured independently by using the transverse boost dependence of $M_{CT}^{\max}$. Section 5 will investigate these techniques with LHC case studies measuring the masses of the top quark, W and neutrino with fully-leptonic $t\bar{t}$ events, and the masses of SUSY particles decaying to a similar final state. Section 6 will conclude.

2. Transformation properties of M_{CT}

2.1 Equal magnitude contra-linear boosts

It is instructive to consider first the transformation properties of M_{CT} under contra-linear equal magnitude boosts, in which δ_1 and δ_2 move in opposite directions with equal momentum. M_{CT} is derived from the quantity M_C given by

$$M_C^2(v_1, v_2) \equiv [E(v_1) + E(v_2)]^2 - [\mathbf{p}(v_1) - \mathbf{p}(v_2)]^2$$
$$= m^2(v_1) + m^2(v_2) + 2[E(v_1)E(v_2) + \mathbf{p}(v_1) \cdot \mathbf{p}(v_2)], \qquad (2.1)$$

and this was shown in Ref. [9] to be invariant under such boosts. By contrast M_{CT} is not in general invariant under such boosts, however the position of the M_{CT} end-point, $M_{CT}^{\max}$, *is*. The reason for this can be understood by observing that one can rewrite Eqn. (2.1) in the following form in the $\delta_1\delta_2$ CoM frame:

$$M_C^2(v_1, v_2) = m^2(v_1) + m^2(v_2) + 2[E_T(v_1)E_T(v_2)\cosh\Sigma\eta(v_i) + \mathbf{p_T}(v_1) \cdot \mathbf{p_T}(v_2)]. \quad (2.2)$$

Comparing with Eqn. (1.1) and noting that $\cosh\Sigma\eta(v_i) \geq 1$ this shows that $M_{CT} \leq M_C$, with equality when $\Sigma\eta(v_i) = 0$. Now M_C, like M_{CT}, is bounded from above by $M_{CT}^{\max}$ and so one finds finally that $M_{CT} \leq M_C \leq M_{CT}^{\max}$. It is interesting to note additionally that M_C equals $M_{CT}^{\max}$ when v_1 and v_2 are co-linear in the δ_i rest frames and hence the necessary and sufficient criteria for $M_{CT} = M_{CT}^{\max}$ are that $\Delta\eta(v_1, v_2) = 0$ and $\Delta\phi(v_1, v_2) = 0$ in the δ_i rest frames while $\Sigma\eta(v_i) = 0$ in the $\delta_1\delta_2$ CoM frame.

A similar argument applies when the transverse mass M_T undergoes co-linear equal magnitude boosts, and the result is similar, namely that M_T is not invariant under arbitrary transverse boosts but nevertheless possesses a boost-invariant end-point. It is interesting to note that in this case the necessary and sufficient conditions for $M_T = M_T^{\max}$ are in some sense the complement of those in the M_{CT} case: here $\Sigma\eta(v_i) = 0$ and $\Delta\phi(v_1, v_2) = \pi$ in the rest frame(s) of the parent particle(s) while $\Delta\eta(v_1, v_2) = 0$ in the event CoM frame. Of course if v_1 and v_2 are the sole products of the decay of the same parent then the first and second criteria are generally satisfied through conservation of momentum.

2.2 Equal magnitude co-linear boosts

The contransverse mass is invariant by construction under co-linear equal magnitude boosts of δ_1 and δ_2 in the beam ($\hat{z}$) direction, by virtue of its dependence purely on transverse quantities. Consequently $M_{CT}^{\max}$ is similarly invariant. In the presence of co-linear equal magnitude boosts in the CoM transverse plane however, equivalent to a single global transverse boost, the values of both M_{CT} and $M_{CT}^{\max}$ can depend on the magnitude and direction of the boost. For instance, when $m(v_1) = m(v_2) = m(v)$ Eqn. (1.3) becomes:

$$M_{CT}^{\max}[m^2(v), p_b] = 2\big(rp_0 + E_0\sqrt{1 + r^2}\big), \qquad (2.3)$$

where $r \equiv p_b/2m(\delta)$, p_b is the net transverse momentum of upstream objects (ISR jets etc.) generating the boost,

$$E_0 \equiv \frac{m^2(\delta) - m^2(\alpha) + m^2(v)}{2m(\delta)}, \qquad (2.4)$$

and $p_0 \equiv \sqrt{E_0^2 - m^2(v)}$.

With sufficient statistics one might hope to use Eqn. (2.3) to measure $m(\delta)$ and $m(\alpha)$ separately by measuring $M_{CT}^{\max}$ as a function of p_b. This possibility is considered further in Section 4. With limited statistics however it would be useful to be able to transform M_{CT} such that its value always lies below the M_{CT} end-point given by Eqn. (1.3). In this case one sacrifices the ability to measure $m(\delta)$ and $m(\alpha)$ independently using the p_b dependence of $M_{CT}^{\max}$ in order to maximise statistics near the $p_b = 0$ M_{CT} end-point, while limiting smearing beyond the end-point due to integration over p_b.

The approach we shall take will involve boosting the four-momenta of the visible decay products v_i back into the $\delta_1 \delta_2$ CoM frame with boost factor β, prior to calculating M_{CT}. If we know neither the sign nor the magnitude of β then the minimum value of M_{CT} that we can obtain by varying the assumed value of β is the one-dimensional analogue of M_{CT} given by M_{Cy} defined by

$$
\begin{aligned}
M_{Cy}^2(v_1, v_2) &\equiv [E_y(v_1) + E_y(v_2)]^2 - [p_y(v_1) - p_y(v_2)]^2 \\
&= m^2(v_1) + m^2(v_2) + 2[E_y(v_1)E_y(v_2) + p_y(v_1)p_y(v_2)],
\end{aligned} \tag{2.5}
$$

where $E_y^2(v_i) \equiv p_y^2(v_i) + m^2(v_i)$ and we have assumed that the boost lies in the $\pm \hat{x}$ direction. M_{Cy} is invariant under arbitrary boosts in the $\hat{x} - \hat{z}$ plane for the same reason that M_{CT} is invariant under boosts in the $\hat{z}$ direction. It represents a conservative lower bound on the value $M_{CT(\text{CoM})}$ of M_{CT} measured in the $\delta_1 \delta_2$ CoM frame. The criterion for M_{CT} to equal M_{Cy} in any given frame, and hence for M_{CT} to be minimised in that frame, is that $A_x = 0$, where A_x is defined by

$$
A_x \equiv p_x(v_1)E_y(v_2) + p_x(v_2)E_y(v_1). \tag{2.6}
$$

As an aside, it is interesting to consider at this point the possibility of using M_C defined by Eqn. (2.1), rather than M_{CT}, and attempting to perform a correction for longitudinal boosts along the beam direction. In this case we know neither the sign nor the magnitude of the z-boost and so by the above argument the appropriate quantity to use is the two-dimensional analogue of M_C, which is just M_{CT} as we have been using already. The criterion for M_C to equal M_{CT} is by analogy with Eqn. (2.6)

$$
p_z(v_1)E_T(v_2) + p_z(v_2)E_T(v_1) = 0, \tag{2.7}
$$

which is equivalent to setting $\Sigma \eta(v_i) = 0$ as required by Eqn. (2.2).

Now in fact we *do* know the sign of the required boost, because we know the direction in the transverse plane of the upstream momentum. Defining this direction to be the $+\hat{x}$ direction we need to boost v_1 and v_2 in this same direction (i.e. use $\beta \geq 0$) to correct for the original boost of the $\delta_1 \delta_2$ CoM frame, which must have been in the $-\hat{x}$ direction. Such a $+\hat{x}$ boost monotonically increases $p_x(v_i)$ and hence monotonically increases the transformed value of A_x towards $+\infty$ as $\beta \to +1$. Let us define now $A_{x(\text{lab})}$ and $M_{CT(\text{lab})}$ to be the values of A_x and M_{CT} measured in the lab frame and A_x' and $M_{CT(\text{corr})}$ to be the equivalent values obtained after boosting v_1 and v_2. If $A_{x(\text{lab})} \geq 0$ then $M_{CT(\text{corr})}$ increases monotonically from $M_{CT(\text{lab})}$ towards $+\infty$ as $\beta \to +1$ (see Figures 1 and 2).
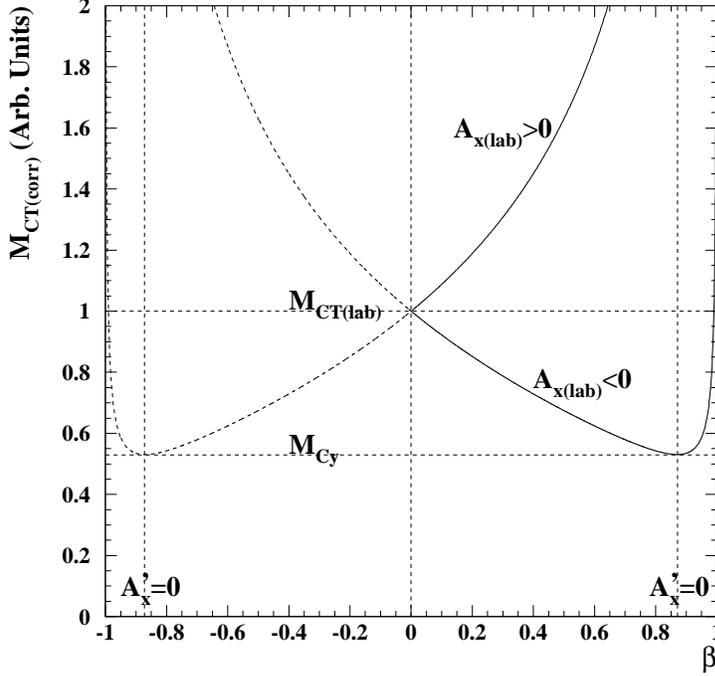
Figure 1: Schematic diagram showing the dependence of $M_{CT(\text{corr})}$ on the boost factor β used in the boost correction. Cases with $A_{x(\text{lab})} > 0$ and $A_{x(\text{lab})} < 0$ are shown. When $\beta \geq 0$ and $A_{x(\text{lab})} \geq 0$ the minimum value of $M_{CT(\text{corr})}$ occurs when $\beta = 0$ and hence $M_{CT(\text{corr})} = M_{CT(\text{lab})}$. If $\beta \geq 0$ and $A_{x(\text{lab})} < 0$ the minimum value of $M_{CT(\text{corr})}$ is M_{Cy}.

Consequently in this case the least conservative lower bound on $M_{CT(\text{CoM})}$ we can obtain is $M_{CT(\text{corr})} = M_{CT(\text{lab})}$. If on the other hand $A_{x(\text{lab})}$ is negative then as β and A'_x increase $M_{CT(\text{corr})}$ first decreases from $M_{CT(\text{lab})}$ towards its minimum value of M_{Cy} (at $A'_x = 0$) before increasing again towards $+\infty$ (see Figures 1 and 2). In this case, without further information, the best we can do is set $M_{CT(\text{corr})} = M_{Cy}$.

Fortunately however we have not yet exhausted the possibilities for boost correction. Observe first that when boosting v_1 and v_2 the boost factor is given by $\beta = p_b/E_{\delta\delta}^{\text{est}}$ where $E_{\delta\delta}^{\text{est}}$ is the assumed value of the energy $E_{\delta\delta}$ of the $\delta_1\delta_2$ CoM frame in the lab frame. Consequently increasing the value of β is equivalent to decreasing $E_{\delta\delta}^{\text{est}}$, and vice versa. Hence if $M_{CT(\text{corr})}$ increases (decreases) monotonically with increasing $E_{\delta\delta}^{\text{est}}$ and we set $E_{\delta\delta}^{\text{est}}$ to a value less than (greater than) $E_{\delta\delta}$, the value of $M_{CT(\text{corr})}$ we obtain provides a conservative lower bound on $M_{CT(\text{CoM})}$. Now if $A_{x(\text{lab})} \geq 0$ then $M_{CT(\text{corr})}$ always increases with increasing β (see Figure 1) and hence it decreases with increasing $E_{\delta\delta}^{\text{est}}$ (see Figure 3 – upper curve). In this case we should set $E_{\delta\delta}^{\text{est}}$ to the upper bound on $E_{\delta\delta}$, boost v_1 and v_2, and obtain a conservative lower bound on $M_{CT(\text{CoM})}$ from the value of $M_{CT(\text{corr})}$ in this frame. If $A_{x(\text{lab})} < 0$ the situation is more complicated (see Figure 3 – lower curve). In this case, if $A'_x < 0$ after boosting with $E_{\delta\delta}^{\text{est}}$ set to both the upper and lower bounds on $E_{\delta\delta}$ then the least conservative lower bound on $M_{CT(\text{CoM})}$ is given by the value of $M_{CT(\text{corr})}$
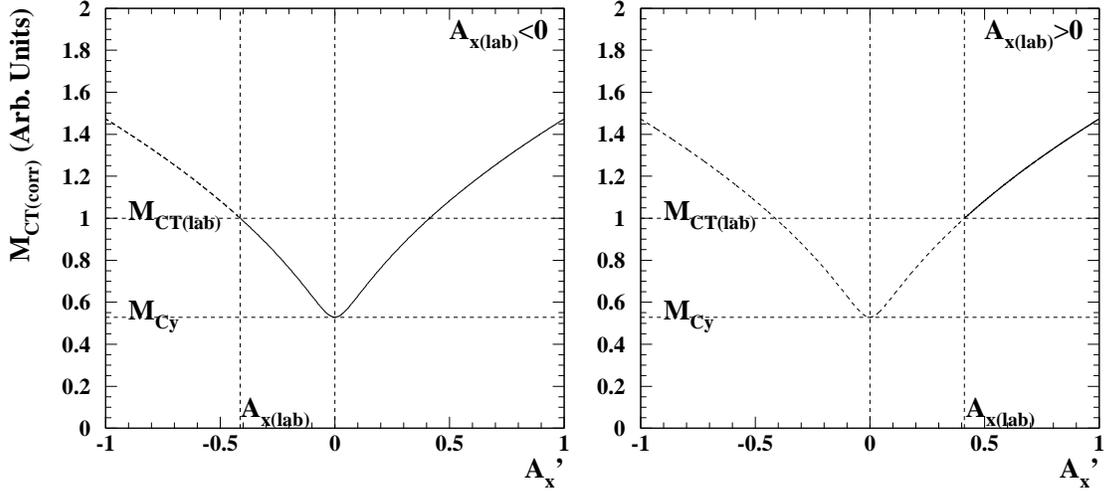
Figure 2: Schematic diagram showing the dependence of $M_{CT(\text{corr})}$ on A'_x. If $A_{x(\text{lab})} < 0$ (left-hand figure) then as A'_x increases from $A_{x(\text{lab})}$, $M_{CT(\text{corr})}$ passes through its minimum at $A'_x = 0$, while if $A_{x(\text{lab})} > 0$ (right-hand figure) it does not.

with $E_{\delta\delta}^{\text{est}}$ set to the lower bound on $E_{\delta\delta}$. Conversely if $A'_x \geq 0$ in both these cases then the least conservative lower bound on $M_{CT(\text{CoM})}$ is given by the value of $M_{CT(\text{corr})}$ with $E_{\delta\delta}^{\text{est}}$ set to the upper bound on $E_{\delta\delta}$. If $A'_x \geq 0$ with $E_{\delta\delta}^{\text{est}}$ set to the lower bound on $E_{\delta\delta}$ but $A'_x < 0$ with $E_{\delta\delta}^{\text{est}}$ set to the upper bound on $E_{\delta\delta}$ then $M_{CT(\text{CoM})}$ could be as low as M_{Cy} and so this should be used as the least conservative lower bound on $M_{CT(\text{CoM})}$.

In fact we can indeed obtain both upper and lower bounds on $E_{\delta\delta}$. An upper bound is provided by the proton-proton centre of mass energy E_{cm} while the total visible energy $\widehat{E}$ of the decay products provides a lower bound. This latter quantity is calculated by summing the energies of the visible decay products with the net transverse momentum of the invisible decay products[1] given by E_T^{miss}. E_T^{miss} equals the total energy of the invisible decay products only when these are massless, co-linear, and moving in the transverse plane, and so in general $\widehat{E} \leq E_{\delta\delta}$. Below we shall denote values of A'_x obtained with $E_{\delta\delta}^{\text{est}}$ set to E_{cm} or $\widehat{E}$ as respectively $A'_{x(\text{lo})}$ and $A'_{x(\text{hi})}$.

Let us now summarise the procedure we have developed for correcting M_{CT} for the effects of co-linear equal magnitude boosts of δ_1 and δ_2 in the transverse plane[2]. First calculate $A_{x(\text{lab})}$ and $A'_{x(\text{lo})}$ using Eqn. (2.6), the latter by boosting v_1 and v_2 with $\beta = p_b/E_{\text{cm}}$. If $A_{x(\text{lab})} \geq 0$ or $A'_{x(\text{lo})} \geq 0$ then one should set $M_{CT(\text{corr})}$ to the boosted value of M_{CT} obtained with $\beta = p_b/E_{\text{cm}}$. If neither of these criteria are satisfied then one should next evaluate $\widehat{E}$ and boost v_1 and v_2 with $\beta = p_b/\widehat{E}$. Now evaluate $A'_{x(\text{hi})}$ using Eqn. (2.6).

---

[1]If a lower bound $m_{\text{lo}}(\alpha)$ on the masses of the individual invisible decay products can be assumed then conservatively one can use $\sqrt{(E_T^{\text{miss}})^2 + 4m_{\text{lo}}^2(\alpha)}$ in $\widehat{E}$ instead of E_T^{miss} to obtain an improved bound on $E_{\delta\delta}$.

[2]f77, C++ and ROOT code implementing this boost-correction procedure can be downloaded from http://projects.hepforge.org/mctlib.
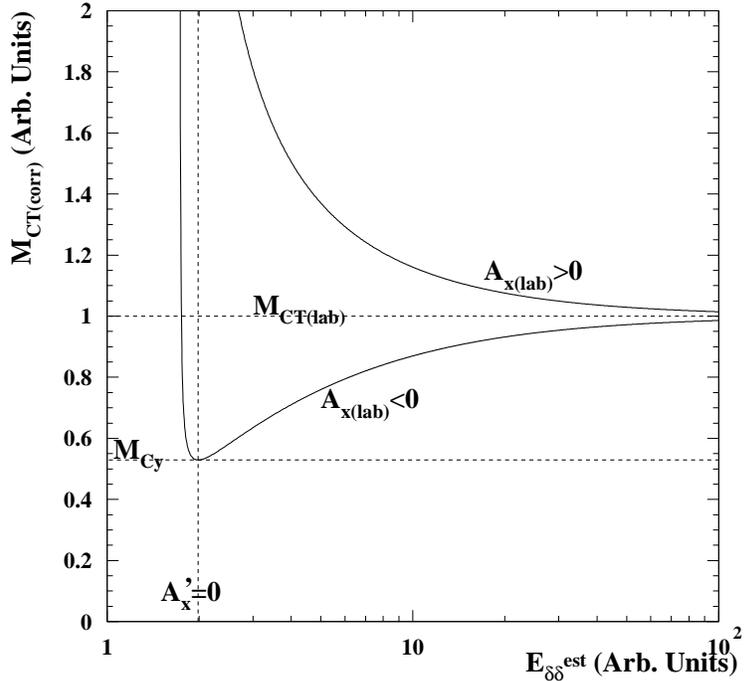
Figure 3: Schematic diagram showing the dependence of $M_{CT(\text{corr})}$ on $E_{\delta\delta}^{\text{est}}$, the estimated value of $E_{\delta\delta}$ used in the boost. Cases with $A_{x(\text{lab})} > 0$ and $A_{x(\text{lab})} < 0$ are shown. When $A_{x(\text{lab})} \geq 0$ or $A'_x > 0$ $M_{CT(\text{lab})}$ decreases with increasing $E_{\delta\delta}^{\text{est}}$. If however $A_{x(\text{lab})} < 0$ and $A'_x < 0$ then $M_{CT(\text{lab})}$ increases with increasing $E_{\delta\delta}^{\text{est}}$.

If $A'_{x(\text{hi})} < 0$ then one should set $M_{CT(\text{corr})}$ to the value of M_{CT} in this boosted frame. If however $A'_{x(\text{hi})} \geq 0$ then one should set $M_{CT(\text{corr})} = M_{Cy}$. An example of the effect of this boost correction procedure is shown in Fig. 4 for the SUSY events considered in Ref. [9].

3. The shape of the M_{CT} distribution

The differences between M_T and M_{CT} identified in Section 2.1 affect the shapes of the distributions of these quantities. As is well-known, M_T possesses a Jacobian peak at $M_T = M_T^{\text{max}}$ when v_1 and v_2 are the sole products of the decay of the same parent. Physically this peak arises because near the end-point all kinematic configurations with different $\eta(v_i)$ generate the same value of M_T, in other words M_T becomes independent of the kinematics of v_1 and v_2.

Turning now to M_{CT}, let us consider first the special case where the $\delta_1\delta_2$ system is not boosted in the laboratory transverse plane and no boost correction is applied. When M_{CT} is calculated for the visible decay products of the $\delta_1\delta_2$ system the extra degrees of freedom resulting from the independent motion of v_1 and v_2 generate a significantly different shape of distribution. Near the end-point at M_{CT}^{max} only events in which both v_1 and v_2 move in the transverse plane can contribute to the distribution. The small probability of this
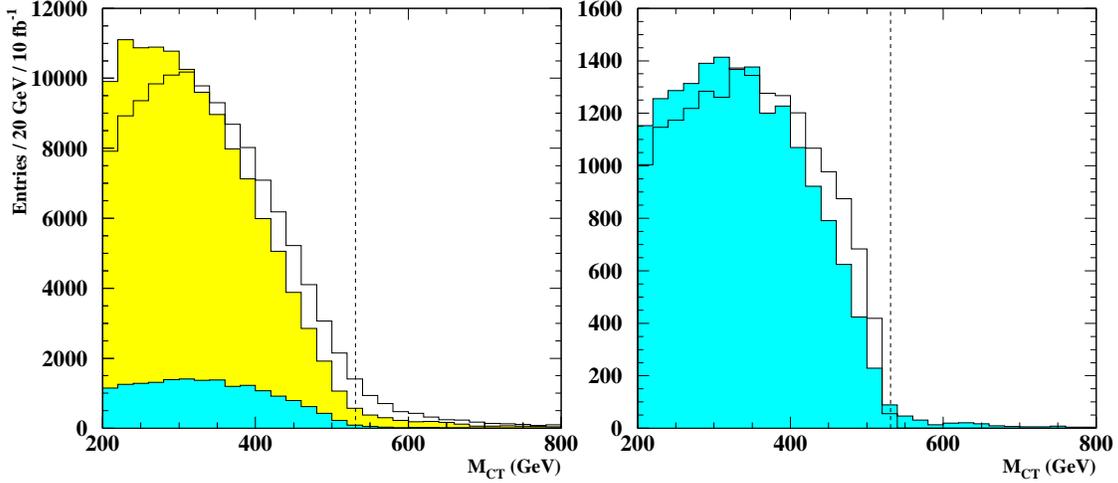
Figure 4: M_{CT} distributions of SUSY events containing at least two jets for the SPS1a benchmark SUSY model considered in Ref. [9]. In the left-hand figure the open histogram shows the M_{CT} distribution with no p_b cut and no correction applied. This diagram should be compared with Figure 2 of Ref. [9] showing the evolution of the uncorrected M_{CT} end-point as a function of the cut on p_b. The light (yellow) histogram shows the M_{CT} distribution of the same events after the co-linear boost correction described in the text has been applied to the M_{CT} values, assuming that all additional jets contribute to the upstream momentum p_b. The medium (cyan) histogram shows the same distribution for $\tilde{q}_R\tilde{q}_R$ pair-production events. In the right-hand figure the latter distribution is plotted on an expanded scale. The open histogram shows the parton-level M_{CT} distribution for the same events. The end-point from $\tilde{q}_R\tilde{q}_R$ pair-production is expected at 531 GeV (denoted by a vertical dashed line in both figures).

configuration (because v_1 and v_2 are uncorrelated) cancels the large probability generated by the Jacobian transformation, resulting in an end-point which tends asymptotically in the absence of boosts to

$$\mathrm{P}(M_{CT})\,\mathrm{d}M_{CT} = A\sqrt{(M_{CT}^{\max})^2 - M_{CT}^2}\,\mathrm{d}M_{CT}, \tag{3.1}$$

where A is a constant. Typical M_{CT} distributions in the absence of boosts, displaying this end-point, are shown in Figure 5.

Despite this cancellation of the peak at $M_{CT}^{\max}$ the M_{CT} distribution can still possess a Jacobian peak. The peak occurs however at the lower limit of the distribution, where $M_{CT} = m(v_1) + m(v_2) \equiv M_{CT}^{\min}$ (see Eqn. (1.1)). The distribution tends asymptotically in the absence of boosts to

$$\mathrm{P}(M_{CT})\,\mathrm{d}M_{CT} = B\frac{M_{CT}}{\sqrt{M_{CT}^2 - (M_{CT}^{\min})^2}}\,\mathrm{d}M_{CT}, \tag{3.2}$$

where B is a constant. This is very similar to the functional form of the M_T Jacobian peak, although in this case it is reversed such that the distribution is real above the peak
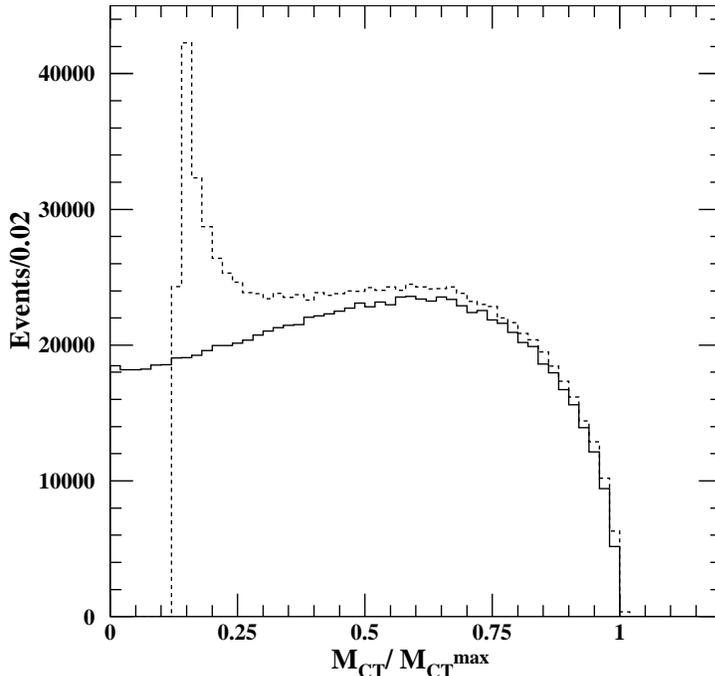
Figure 5: Typical M_{CT} distributions in the absence of boosts for massless visible particles (full histogram) and massive visible particles of total mass $0.13M_{CT}^{\max}$ (dashed histogram). The x-axis has been scaled such that the end-point lies at $M_{CT}/M_{CT}^{\max} = 1$.

rather than below it. Physically the peak occurs because when $M_{CT} \sim M_{CT}^{\min}$ the value of M_{CT} becomes independent of the kinematics of v_1 and v_2, because the $m(v_i)$ terms in Eqn. (1.1) dominate. Hence all kinematic configurations generate similar values of M_{CT}. An example of such a peak can be seen in the dashed histogram in Figure 5. Note that when $M_{CT}^{\min} = 0$ the numerator and denominator in Eqn. (3.2) cancel leaving a uniform distribution (see e.g. full histogram in Figure 5).

Consider now the general case where the $\delta_1\delta_2$ system has been boosted in the laboratory transverse plane, and the boost correction procedure discussed in Section 2.2 has been applied. In this case there can be a further enhancement of the population of events at $M_{CT} = M_{CT}^{\min}$. If $A_{x(\text{lab})} < 0$ and $A'_{x(\text{hi})} > 0$ then the boost-corrected value of M_{CT} is given by M_{Cy} from Eqn. (2.5). If the tranverse momenta of the two visible particles under consideration are bisected by the boost direction however, then M_{Cy} can take very small values, even if the transverse momenta of the v_i particles are relatively large. This effect is particularly striking when $m(v_1) = m(v_2) = M_{CT}^{\min} = 0$, in which case it is straightforward to see from Eqn. (2.5) that $M_{Cy} = 0$. We shall refer below to the resulting peak at $M_{CT} = M_{CT}^{\min}$ as the '$M_{CT} = M_{Cy}$' peak.

Specific examples of the peaks and end-points discussed in this section can be seen in Section 5 below.

4. Measuring $m(\delta)$ and $m(\alpha)$ independently

The dependence of $M_{CT}^{\max}$ on $m(v_i)$, noted in Ref. [9], and on p_b, noted in Section 2.2, provides potential techniques for measuring $m(\delta)$ and $m(\alpha)$ independently. In this section we develop these techniques in more detail.

4.1 Using the $m(v_i)$ dependence of $M_{CT}^{\max}$

As remarked in Section 1, when attempting to measure $m(\delta)$ and $m(\alpha)$ independently using Eqn. (1.3) the requirement $m(v_1) = m(v_2) = m(v)$ reduces significantly the event selection efficiency. One can consider ameliorating this problem by removing this mass equality requirement and considering the dependence of the resulting M_{CT} end-point on both $m^2(v_1)$ and $m^2(v_2)$. This is given by

$$
\left(M_{CT}^{\max}[m^2(v_1), m^2(v_2)] \right)^2 = m^2(v_1) + m^2(v_2) + 2 \Big(E_0(v_1) E_0(v_2)
$$
$$
+ \sqrt{\left[E_0^2(v_1) - m^2(v_1) \right] \left[E_0^2(v_2) - m^2(v_2) \right]} \Big), \quad (4.1)
$$

where

$$
E_0(v_i) \equiv \frac{m^2(\delta) - m^2(\alpha) + m^2(v_i)}{2m(\delta)}. \quad (4.2)
$$

In this case all events passing background rejection cuts are used, however the implicit requirement of binning in both $m^2(v_1)$ and $m^2(v_2)$ to measure $M_{CT}^{\max}[m^2(v_1), m^2(v_2)]$ still limits the available event statistics in each end-point measurement (modulo the symmetry under interchange of v_1 and v_2 of $M_{CT}^{\max}[m^2(v_1), m^2(v_2)]$). As an aside, Eqn. (4.1) provides a link between the 'stransverse mass' $M_{T2}(\chi)$ [1] and M_{CT}. This is discussed in more detail in Appendix A.

An alternative to using Eqn. (4.1) for measuring $m(\delta)$ and $m(\alpha)$ independently involves observing that $M_{CT}^{\max}[m^2(v)]$ is linearly dependent on $m^2(v)$ in Eqn. (1.3) and hence that

$$
M_{CT}^{\max}[m_{\max}^2] = \max \left(M_{CT}^{\max}[m^2(v_1)], M_{CT}^{\max}[m^2(v_2)] \right), \quad (4.3)
$$

where,

$$
m_{\max} \equiv \max \left(m(v_1), m(v_2) \right). \quad (4.4)
$$

Then we can make use of the following inequality:

$$
M_{CT}^{\max}[m^2(v_1), m^2(v_2)] \leq M_{CT}^{\max}[m_{\max}^2], \quad (4.5)
$$

to find that

$$
M_{CT}(v_1, v_2) \leq M_{CT}^{\max}[m^2(v_1), m^2(v_2)] \leq M_{CT}^{\max}[m_{\max}^2]. \quad (4.6)
$$

Consequently if the two-dimensional distribution of event $M_{CT}(v_1, v_2)$ values versus event $m_{\max}^2$ values is plotted, for all events passing background rejection cuts, the distribution will display an M_{CT} end-point dependence on $m_{\max}^2$ given by:

$$
M_{CT}^{\max}[m_{\max}^2] = \frac{m_{\max}^2}{m(\delta)} + \frac{m^2(\delta) - m^2(\alpha)}{m(\delta)}. \quad (4.7)
$$

Hence $m(\delta)$ and $m(\alpha)$ may be obtained by measuring the gradient and intercept of the end-point dependence on $m_{\max}^2$ in a similar manner to the existing technique using Eqn. (1.3). Now however all events passing the background rejection cuts can be used rather than just a small subset.

It should be noted here that although this technique is sound from a theoretical point-of-view, the uneven distribution of events in the $M_{CT}(v_1, v_2)$ versus $m_{\max}^2$ plane can cause difficulty when attempting to use it in practice. This is discussed further in Section 5.

4.2 Using the p_b dependence of $M_{CT}^{\max}$

In Section 2.2 we developed a procedure for correcting $M_{CT}(v_1, v_2)$ such that it is always bounded from above by the expression for $M_{CT}^{\max}$ obtained when the upstream momentum $p_b = 0$. Given sufficient statistics however an alternative procedure would involve binning the non-boost-corrected value of $M_{CT}(v_1, v_2)$ in p_b and measuring $m(\delta)$ and $m(\alpha)$ independently from the dependence of $M_{CT}^{\max}$ on p_b. When $m(v_1) = m(v_2) = m(v)$ this dependence is given by Eqn. (2.3), however we can also obtain a general expression valid even when $m(v_1) \neq m(v_2)$, which is

$$\left(M_{CT}^{\max}[m^2(v_1), m^2(v_2), p_b] \right)^2 = \left(M_{CT}^{\max}[m^2(v_1), m^2(v_2)] \right)^2 +$$
$$4r^2 \left(E_0(v_1) E_0(v_2) + p_0(v_1) p_0(v_2) + \frac{1}{r}\sqrt{1 + r^2} \left[p_0(v_1) E_0(v_2) + p_0(v_2) E_0(v_1) \right] \right), \quad (4.8)$$

where $M_{CT}^{\max}[m^2(v_1), m^2(v_2)]$ is obtained from Eqn. (4.1), $r \equiv p_b/2m(\delta)$, $E_0(v_i)$ is given by Eqn. (4.2) and $p_0(v_i) \equiv \sqrt{E_0^2(v_i) - m^2(v_i)}$. In principle the additional dependence of $M_{CT}^{\max}$ on the angle between the p_b vector and the net momentum of v_1 and v_2 in the transverse plane could also be exploited, although this is not considered further here.

The advantage of using the p_b dependence of $M_{CT}^{\max}$ rather than the $m(v_i)$ dependence discussed in Section 4.1 is that $m(\delta)$ and $m(\alpha)$ can in principle be measured independently even when $m(v_1) = m(v_2) = m(v) \simeq 0$, for instance when the v_i particles are jets or leptons. This avoids potential combinatorial problems inherent in the latter technique. In this special case the expression for $M_{CT}^{\max}$ becomes

$$M_{CT}^{\max}[0, 0, p_b] = M_{CT}^{\max}[0, 0, 0] \left(r + \sqrt{1 + r^2} \right). \quad (4.9)$$

A toy Monte Carlo example $M_{CT}(v_1, v_2)$ versus p_b distribution for massless v_i particles is shown in Figure 6 together with the theoretical bound from Eqn. 4.9.

As with the use of the $m(v_i)$ dependence of $M_{CT}^{\max}$ in Section 4.1 the above technique is sound from a theoretical perspective, however as we shall see in Section 5 the uneven distribution of events in the $M_{CT}(v_1, v_2)$ versus p_b plane can cause difficulty when attempting to use it in practice.

5. Mass measurement for two-step decay chains

5.1 Generic strategy

We shall now investigate the use of the boost-corrected contransverse mass discussed in Section 2.2 (hereafter referred to simply as M_{CT}) to measure the masses of pair-produced
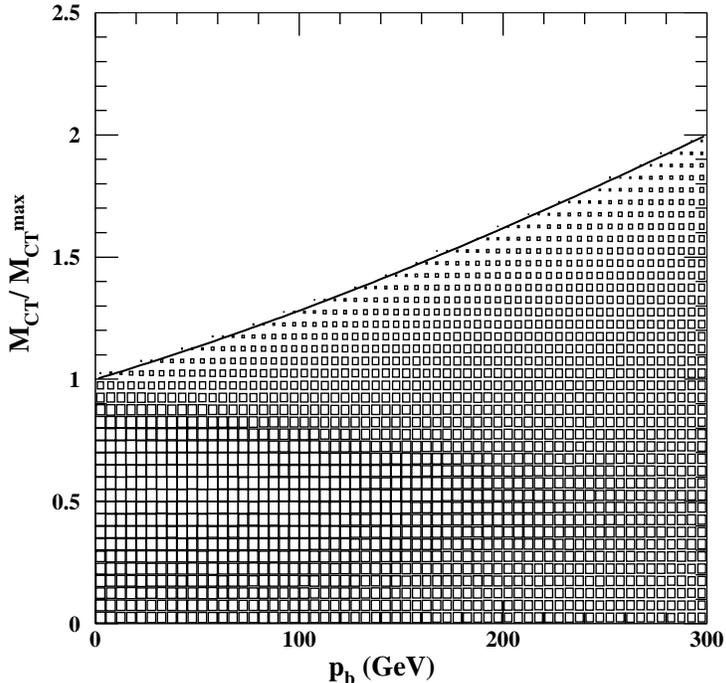
Figure 6: Example $M_{CT}(v_1, v_2)$ versus p_b distribution generated with a toy Monte Carlo showing the dependence of $M_{CT}^{\max}$ on p_b given by Eqn. (4.9). The simulated events consist of pair-produced δ particles of mass 200 GeV, each decaying into a massless visible particle and an invisible particle α of mass 100 GeV. p_b is evenly distributed in the range 0–300 GeV. The $M_{CT}(v_1, v_2)$ axis has been normalised to $M_{CT}^{\max}$ obtained when $p_b = 0$.

heavy particles decaying via symmetric two-step sequential two-body decay chains. As discussed in Ref. [14] mass measurement with such chains is non-trivial because they are too short to solve fully for the masses using invariant mass end-point techniques [20, 21, 22, 23, 24] or the 'mass relation' method [25]. The decay chains considered can be written in the form:

$$\delta \to P\beta \to PQ\alpha, \tag{5.1}$$

where δ, β and α are generic massive particles, P and Q are generic visible particles (here assumed massless) and α is invisible. The two chains present in each event can be seen in diagrammatic form in Figure 7, where particles appearing in the second decay chain are denoted with primed labels. We assume in the following discussion that particles labeled with the same letter possess the same mass.

With each event we can construct one pair of invariant mass observables and three contransverse mass observables from the momenta of the four observed particles P, Q, P' and Q'. These observables are:

- $m(P^{(\prime)}, Q^{(\prime)})$: the invariant masses of the visible products of the two decay chains

- $M_{CT}(P, P')$: M_{CT} constructed from the momenta of P and P'

- $M_{CT}(Q, Q')$: M_{CT} constructed from the momenta of Q and Q'

- $M_{CT}([PQ], [P'Q'])$: M_{CT} constructed from the momenta of the aggregate products of each chain $[PQ]$ and $[P'Q']$.

These observables possess kinematic end-points whose positions are functions of the masses $m(\delta)$, $m(\beta)$ and $m(\alpha)$. The end-point positions are respectively[3]:

$$m^{\max}(P, Q) = \frac{\sqrt{[m^2(\delta) - m^2(\beta)][m^2(\beta) - m^2(\alpha)]}}{m(\beta)} \equiv k_1, \tag{5.2}$$

$$M_{CT}^{\max}(P, P') = \frac{m^2(\delta) - m^2(\beta)}{m(\delta)} \equiv k_2, \tag{5.3}$$

$$M_{CT}^{\max}(Q, Q') = \frac{m^2(\beta) - m^2(\alpha)}{m(\beta)} \equiv k_3, \tag{5.4}$$

$$M_{CT}^{\max}([PQ], [P'Q']) = \frac{m^2(\delta) - m^2(\beta)}{m(\delta)} + m(\delta) \left(\frac{m^2(\beta) - m^2(\alpha)}{m^2(\beta)} \right) \equiv k_4, \tag{5.5}$$

where the final relationship is obtained from Eqn. (1.3) with $m(v) = m^{\max}(P, Q)$. In addition the two-dimensional distribution of events in the $M_{CT}([PQ], [P'Q'])$ versus $m_{\max}^2$ plane discussed in Section 4.1 can be constructed, providing additional mass constraints via Eqn. (4.7). The two-dimensional distributions of events in the (non-boost-corrected) $M_{CT}(P, P')$ versus p_b and $M_{CT}(Q, Q')$ versus p_b planes discussed in Section 4.2 can also in principle be used.

Using Eqns. (5.2), (5.3) and (5.4) the mass of the parent particle δ can be calculated from:

$$m(\delta) = \frac{k_1^4 k_2}{k_1^4 - k_2^2 k_3^2}. \tag{5.6}$$

The masses of β and α can then be obtained by simple substitution into Eqns. (5.3) and (5.4) respectively. The constraints on the masses provided by Eqn. (4.7), Eqn. (5.5) and/or Eqn. (4.8) may be more difficult to exploit, as shall be discussed in Section 5.2, but they can be used as a closure test for the masses measured using the other constraints.

In typical SUSY decay chains we consider cases where the particles P and Q can be either quarks/jets (q) or leptons (ℓ), leading to the following possible final-state configurations: $\{P \equiv q, Q \equiv q\}$, $\{P \equiv q, Q \equiv \ell\}$ and $\{P \equiv \ell, Q \equiv \ell\}$. The second of these configurations is particularly favourable from an experimental point-of-view because in this case there is no ambiguity in assigning particles to steps in the decay chains when constructing $M_{CT}(P, P')$ and $M_{CT}(Q, Q')$. In the case-studies presented below we shall therefore focus on events with the final state $P \equiv q$ and $Q \equiv \ell$.

---

[3]When dealing with single-step three-body decay chains in which two visible particles and one invisible particle are produced in each decay Eqns. (5.2)–(5.5) are replaced by $m^{\max}(P, Q) = m(\delta) - m(\alpha)$, $M_{CT}^{\max}([PQ], [P'Q']) = 2[m(\delta) - m(\alpha)]$ and $M_{CT}^{\max}(P, P') = M_{CT}^{\max}(Q, Q') = [m^2(\delta) - m^2(\alpha)]/m(\delta)$, although in the last two cases the distributions are strongly phase-space suppressed near the endpoints.
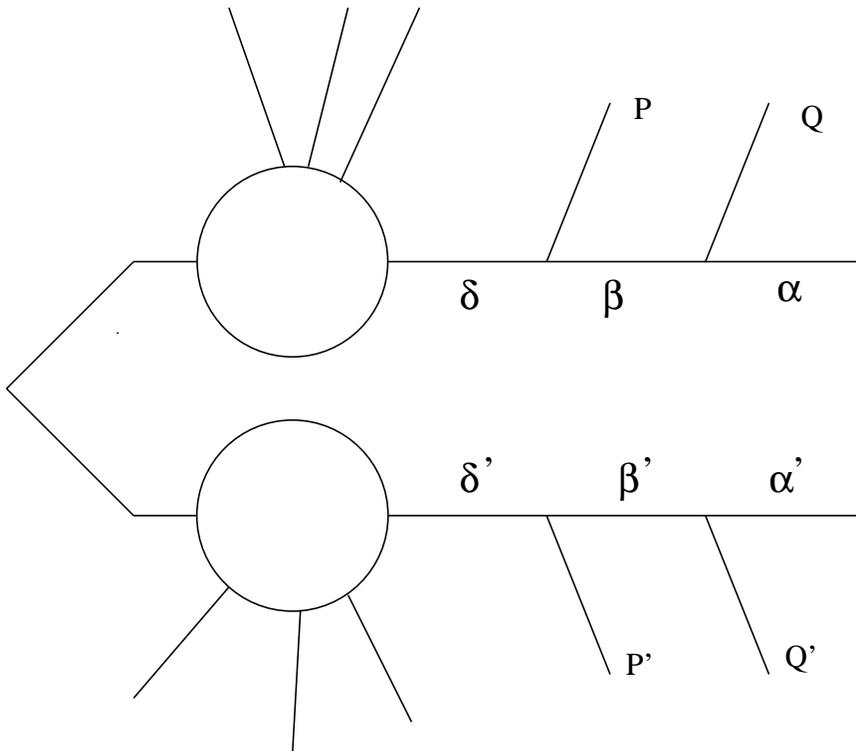
Figure 7: Diagrammatic view of the decay chain described in the text. The mass measurement technique described in the text is independent of the boost given to the system of interest by upstream decays or ISR (denoted by circles).

5.2 Benchmarking on top events

The mass measurement technique proposed above can be tested with $t\bar{t}$ events in which both top quarks decay to leptons via leptonically decaying W's through the chain:

$$t \to bW \to b\ell\nu. \tag{5.7}$$

Such events contain two symmetric two-step sequential two-body decay chains, with invisible particles being produced at the end of each chain. They therefore provide a suitable testbed for our mass measurement technique, with $\delta \equiv t$, $\beta \equiv W$, $\alpha \equiv \nu$, $P \equiv b$ and $Q \equiv \ell$. The main notable difference between these events and SUSY events is that the invisible particles are in reality approximately massless, however in our analysis we shall not make this assumption. This approach has been used previously to study alternative SUSY particle mass measurement techniques [18, 14].

In order to evaluate the observables discussed in Section 5.1, we generated with `MC@NLO 3.3` [26, 27] an inclusive sample of $\sqrt{s} = 14$ TeV LHC $t\bar{t}$ events with an input top mass of 172.5 GeV. The events were passed through the parameterised detector simulation `ACERDET` [28] which was modified to reproduce the resolutions for leptons and jets given in [29]. For the tagging of b-jets, an efficiency of 60% was assumed, for a light jet rejection of 100. The total generated sample was 2.2 M events, corresponding to an integrated luminosity of approximately 3 fb^{-1}.

Events were selected with the following requirements:

1. $N_{\text{jet}} \geq 2$, with $p_T(j_2) > 40$ GeV

2. $E_T^{miss} > 30$ GeV

3. $N_{\text{lep}} = 2$, where lep $= e/\mu$(isolated) and $p_T(l_2) > 20$ GeV

4. At least two jets tagged as b with $p_T > 50$ GeV

5. Only one of the two possible sets of pairings of the two leptons with the two leading b-jets should generate invariant mass values which are both less than 175 GeV. This cut was intended to reduce the experimental combinatorial background and was used only when constructing observables which required the pairing of leptons and jets from the same decay chain.

Approximately 16100 (8300) events passed cuts 1-4 (1-5) respectively. Of these 15200 (7400) were indeed events in which both hard W's decayed into a muon or electron. The remaining events contained at least one tau lepton decaying leptonically into e or μ.

With the two $b\ell$ pairs, each corresponding to the decay of a different top quark, one can construct the observables discussed in Section 5.1. These observables are $m(b^{(\prime)}, \ell^{(\prime)})$, $M_{CT}(b, b')$, $M_{CT}(\ell, \ell')$ and $M_{CT}([b\ell], [b'\ell'])$. Neglecting the mass of the b-quark, the end-points in the distributions of these quantities lie at (from Eqns. (5.2)–(5.5)):

$$m^{\max}(b, \ell) = \frac{\sqrt{[m^2(t) - m^2(W)][m^2(W) - m^2(\nu)]}}{m(W)} = 152.6 \text{ GeV}, \tag{5.8}$$

$$M_{CT}^{\max}(b, b') = \frac{m^2(t) - m^2(W)}{m(t)} \equiv 135.0 \text{ GeV}, \tag{5.9}$$

$$M_{CT}^{\max}(\ell, \ell') = \frac{m^2(W) - m^2(\nu)}{m(W)} \equiv 80.4 \text{ GeV}, \tag{5.10}$$

$$M_{CT}^{\max}([b\ell], [b'\ell']) = \frac{m^2(t) - m^2(W)}{m(t)} + m(t)\left(\frac{m^2(W) - m^2(\nu)}{m^2(W)}\right) \equiv 307.5 \text{ GeV}. \tag{5.11}$$

Accounting for $m(b) \neq 0$ translates into shifts of less than 0.1% in the end-point positions.

We show in Figure 8 the distributions of the observables at parton-level and at detector-level for events passing the selection cuts in which both W's decay into electron and muons. All contransverse mass observables have been corrected for transverse boosts according to the procedure discussed in Section 2.2. It can be seen that the end-point structures at parton-level are conserved at detector-level, modulo some smearing. The enhancement observed at the lower limit of the $M_{CT}(b, b')$ distribution is generated by the Jacobian peak at $M_{CT} = M_{CT}^{\min} = 2m(b)$ discussed in Section 3 together with the $M_{CT} = M_{Cy}$ effect of the boost correction procedure discussed in the same ssection. The $M_{CT}(\ell, \ell')$ distribution in Figure 8 is relatively unaffected by the Jacobian enhancement because $M_{CT}^{\min} = 0$ for massless leptons. The dilepton systems in these events receive large boosts from the bb' recoil however and so the boost correction procedure generates a prominent $M_{CT} = M_{Cy}$ peak at $M_{CT} = 0$.
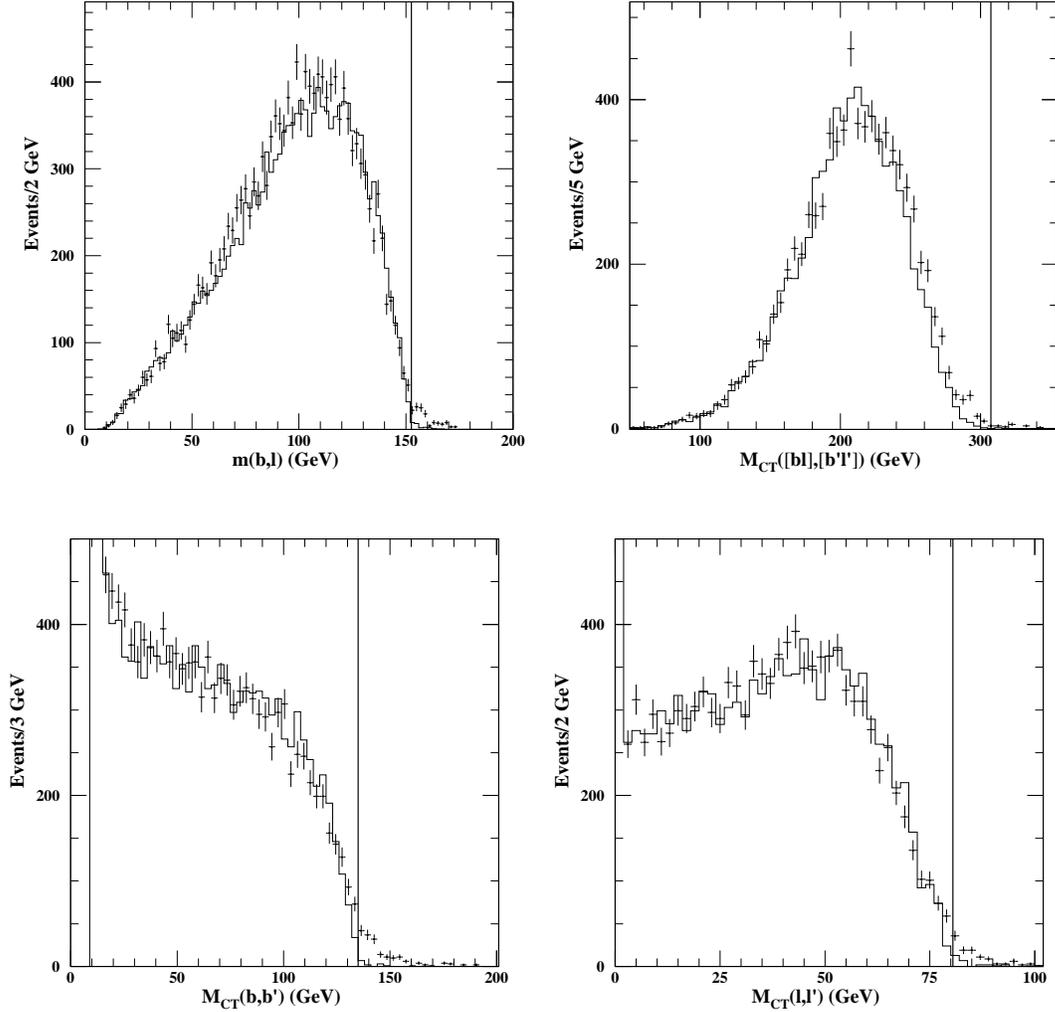
Figure 8: Distributions of $m(b^{(\prime)}, \ell^{(\prime)})$ (top-left), $M_{CT}([b\ell], [b'\ell'])$ (top-right), $M_{CT}(b, b')$ (bottom-left) and $M_{CT}(\ell, \ell')$ (bottom-right) for $t\bar{t}$ events passing the selection cuts where both leptons are generated directly from a W decay. The histograms show the parton-level distributions while the points with error-bars show the distributions after detector-level smearing. The expected end-point positions are indicated with vertical lines. The small populations of parton-level events lying beyond the expected end-points arise from the natural width of the W.

In order to explore in an approximate manner the potential precision of mass measurements obtained with this technique, we fit the end-points of the distributions with a linear function smeared by detector resolution effects. Following Ref. [29] we use a function $f(x)$ given by:

$$f(x) = \frac{1}{\sqrt{2\pi}\sigma} \int_0^{x^{\mathrm{EP}}} \exp\left(-\frac{(x - x')^2}{2\sigma^2}\right) \max\{A(x' - x^{\mathrm{EP}}), 0\} \, dx' + a + bx. \qquad (5.12)$$

Here x is the observable under consideration, x^{EP} represents the end-point position, σ represents the resolution of the assumed gaussian detector smearing, A is the slope of the
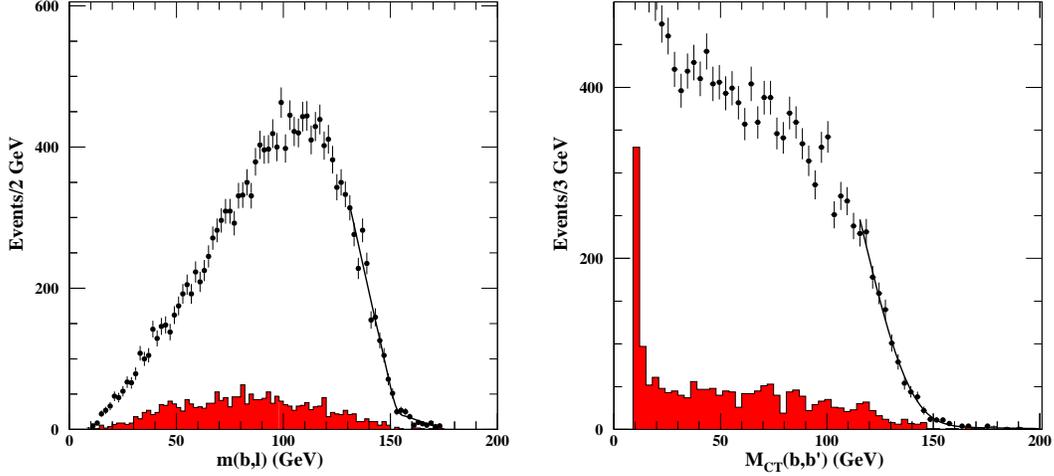
Figure 9: Distributions of $m(b^{(\prime)}, \ell^{(\prime)})$ (left) and $M_{CT}(b, b')$ (right) at detector-level for $t\bar{t}$ events passing the selection cuts. The dark (red) histogram indicates the distribution of events passing the selection where one of the two leptons is not directly produced in the decay of a W. The fit to the end-point function described in the text is shown.
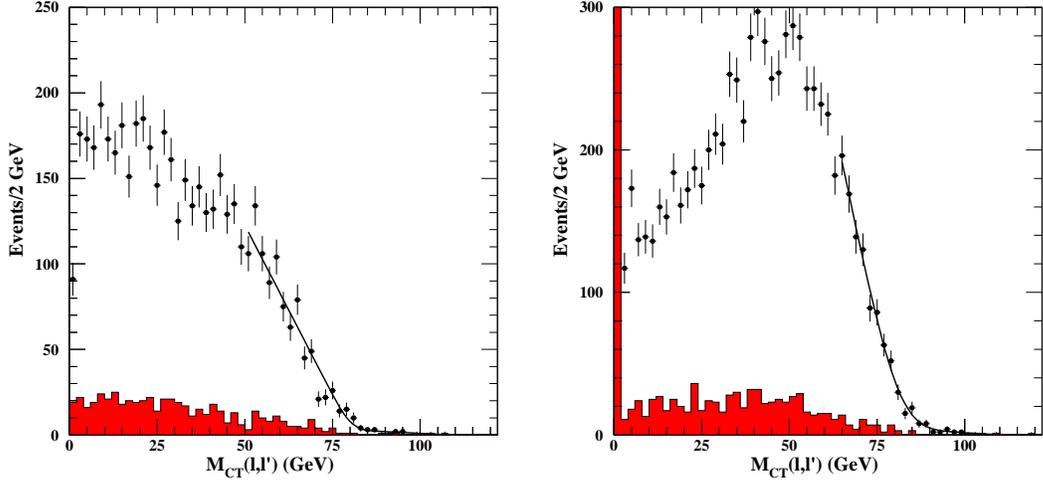
Figure 10: Distributions of $M_{CT}(\ell, \ell')$ for $A_{x(\mathrm{lab})} > 0$ (left), and $A_{x(\mathrm{lab})} < 0$ (right) at detector-level for $t\bar{t}$ events passing the selection cuts. The dark (red) histogram indicates the distribution of events passing the selection where one of the two leptons is not directly produced in the decay of a W. The fit to the end-point function described in the text is shown.

distribution before smearing, and a and b are parameters describing an assumed linear background distribution. The latter distribution helps to take into account the effects of both combinatorial background from incorrect assignment of visible particles to decay chains and non-gaussian tails in the experimental resolution.

For the observables $m(b^{(\prime)}, \ell^{(\prime)})$ and $M_{CT}(b, b')$, the fits to the distributions for all

detector-level events passing the cuts are shown in Figure 9, with the irreducible background of $t\bar{t}$ events where at least one of the leptons is not directly produced in a W decay shown in grey (red). The fit function reproduces well the observed shape, and the value of the resolution parameter σ obtained from the fit is in good agreement with the actual value of the smearing used in the detector simulation.

The situation is somewhat more complex for the $M_{CT}(\ell, \ell')$ observable. In this case one has two populations. If $A_{x(\text{lab})} > 0$ only a very small transverse boost correction is applied to M_{CT}, using $E_{\delta\delta}^{\text{est}} = E_{\text{cm}}$. Therefore the experimental end-point resolution is to a good approximation just the resolution of the lepton p_T measurement (of order 1 GeV), plus the end-point smearing arising from the W natural width (of order 2-3 GeV). If $A_{x(\text{lab})} < 0$ however, M_{CT} is corrected using the p_T of the hadronic recoil, resulting in a significantly larger resolution of order 9-10 GeV. The two configurations must therefore be fitted separately. The distributions are shown in Figure 10, for $A_{x(\text{lab})} > 0$ ($A_{x(\text{lab})} < 0$) on the left (right). From the figure one can also observe that the gradient of the $A_{x(\text{lab})} > 0$ distribution near the end-point is smaller, and it was necessary in this case to fix the experimental resolution to 3 GeV in order to obtain an acceptable fit.

Measurement of the end-point in the $M_{CT}([b\ell], [b'\ell'])$ distribution presents further
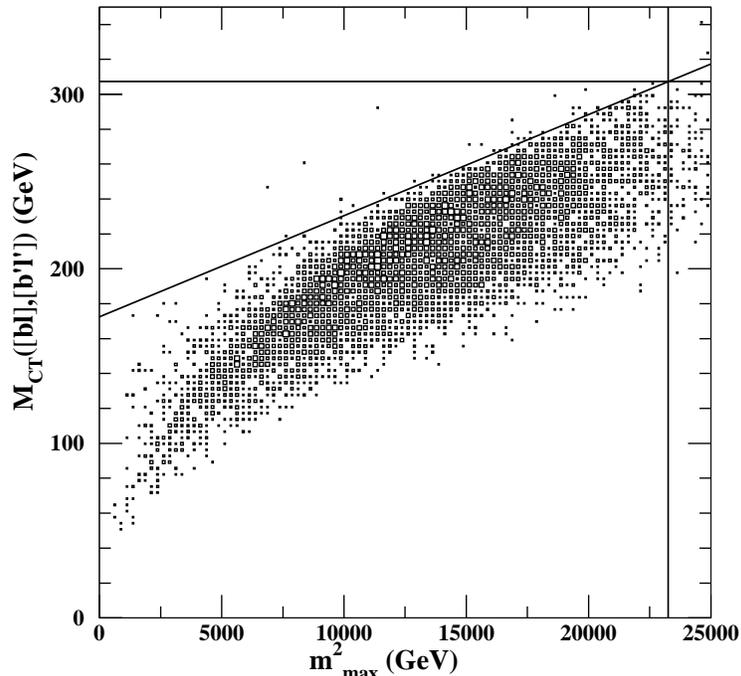
Figure 11: Two-dimensional distribution in the $M_{CT}([b\ell], [b'\ell'])$ versus m_{max}^2 plane of detector-level $t\bar{t}$ events passing the selection cuts. The extremal values of the two observables, given by Eqns. (5.11) and (5.8) are denoted by horizontal and vertical lines respectively. The dependence of $M_{CT}^{\text{max}}([b\ell], [b'\ell'])$ on m_{max}^2 given by Eqn. (4.7) is denoted by the diagonal line.
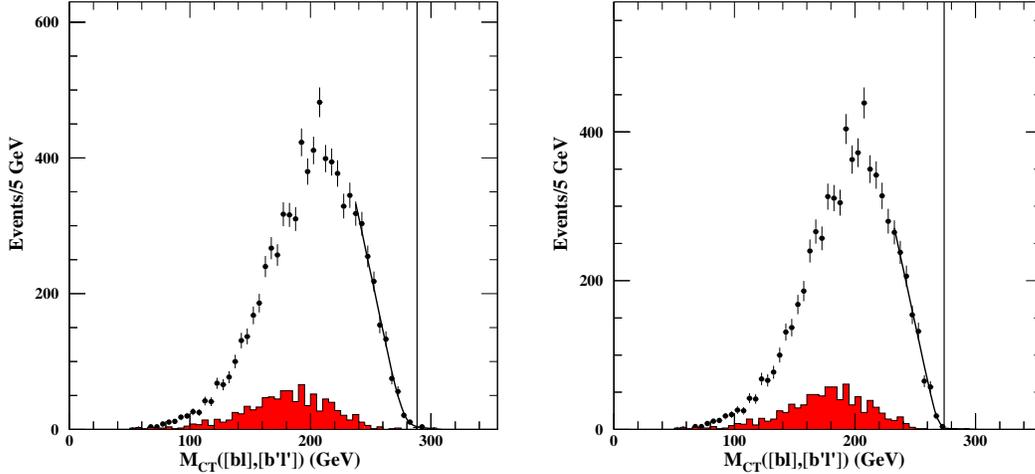
Figure 12: Distributions of $M_{CT}([b\ell], [b'\ell'])$ for detector-level $t\bar{t}$ events passing the selection cuts after requiring additionally that $m_{\max}^2 < 20000$ GeV^2 (left) and $m_{\max}^2 < 17500$ GeV^2 (right). The vertical lines indicate the expected end-point positions.

challenges due to the concave shape of the distribution near to the end-point, seen in Figure 8(top-right). For this end-point the assumption of a linear shape breaks down, primarily due to the depopulation of the $M_{CT}([b\ell], [b'\ell'])$ versus $m_{\max}^2$ plane near $m_{\max}^2 = (m^{\max}(b, \ell))^2$ seen in Figure 11. An alternative strategy for constraining the masses with $M_{CT}([b\ell], [b'\ell'])$ would be to measure the dependence of $M_{CT}^{\max}([b\ell], [b'\ell'])$ on $m_{\max}^2$, as discussed in Section 4.1. This could be accomplished in practice by constructing $M_{CT}([b\ell], [b'\ell'])$ histograms of those events which pass a cut on $m_{\max}^2$. Unfortunately however this procedure is also complicated by the presence of concave end-points, as can be seen in Figure 12. Further progress with this specific element of the contransverse mass technique will likely require a dedicated study of end-point shapes, which is outside of the scope of this paper. Because of these considerations we will not use the measurements of $M_{CT}^{\max}([b\ell], [b'\ell'])$ in the following mass measurement study. Nevertheless such constraints could be useful for validating mass measurements obtained from the other observables. Similar considerations apply when attempting to use the non-boost-corrected $M_{CT}(b, b')$ and $M_{CT}(\ell, \ell')$ observables to measure the dependence of $M_{CT}^{\max}(b, b')$ and $M_{CT}^{\max}(\ell, \ell')$ on p_b, as shown in Figure 13, and this technique will also not be considered further here.

The results of the end-point fits are listed in Table 1, where the first uncertainty is the statistical uncertainty from the MINUIT [30] fitting program for the chosen fit interval, the second is the systematic uncertainty obtained by varying the fit interval and the third uncertainty is the correlated systematic uncertainty derived from assumed energy scale uncertainties of 1% for b-jets and 0.1% for leptons [31]. The quoted uncertainties should be considered approximate and could be improved with the use of better end-point fitting functions, for instance templates derived from Monte Carlo simulation studies.

Based on the end-point measurement uncertainties listed in Table 1 it is possible to
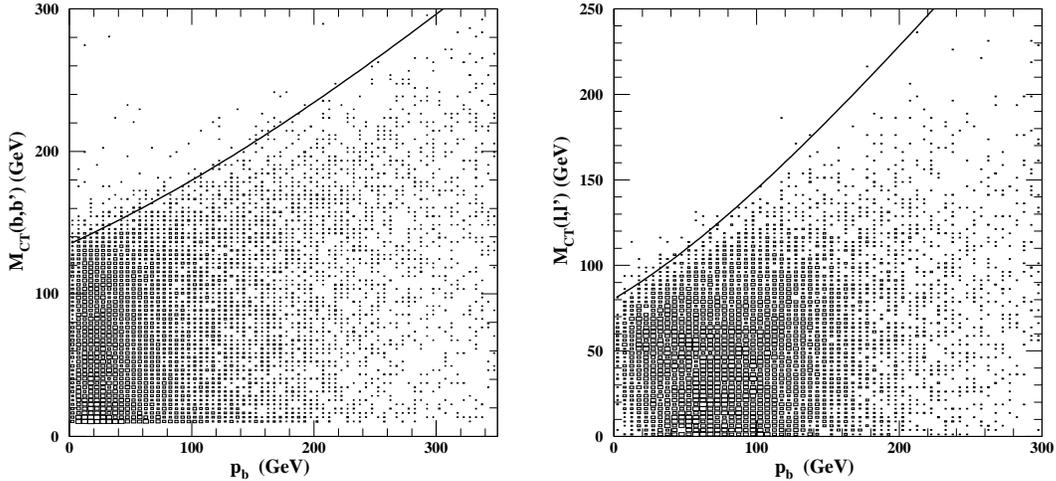
Figure 13: Two-dimensional distributions in the $M_{CT}(b, b')$ versus p_b plane (left) and $M_{CT}(\ell, \ell')$ versus p_b plane (right) of detector-level $t\bar{t}$ events passing the selection cuts. The dependence of $M_{CT}^{\max}$ on p_b given by Eqn. (4.9) is denoted by the curved line in each case. The small population of events lying beyond $M_{CT}^{\max}$ in the left-hand figure arises from the finite detector-level b-jet energy resolution, which degrades at lower energy.

End-point	Truth (GeV)	Measured (GeV)
$m^{\max}(b, \ell)$	152.6	$152.8 \pm 1.7 \pm 1 \pm 0.8$
$M_{CT}^{\max}(b, b')$	135.0	$137.7 \pm 3.6 \pm 3 \pm 1.4$
$M_{CT}^{\max}(\ell, \ell')$ $(A_{x(\text{lab})} < 0)$	80.4	$80.2 \pm 0.5 \pm 1 \pm 0.1$
$M_{CT}^{\max}(\ell, \ell')$ $(A_{x(\text{lab})} > 0)$	80.4	$81.2 \pm 1.7 \pm 2 \pm 0.4$

Table 1: End-point positions in GeV. The first uncertainty is statistical, while the second and third are respectively the uncorrelated systematic and correlated energy scale uncertainties. The expected end-point positions from Eqns. (5.8), (5.9) and (5.10) are listed in the column labelled 'Truth'. The assumed integrated luminosity is 3 fb^{-1}.

evaluate the achievable precisions for measuring the masses of the top quark, W and neutrino. We use the technique described in Ref. [32], where for each end-point measurement we generate a set of pseudo-experiments by sampling from a gaussian distribution centred on the nominal value of the end-point position of width equal to the estimated measurement precision. We assume that the measurements are uncorrelated with the exception of the energy scale uncertainties, which are assumed to be fully correlated. For each pseudo-experiment we calculate the value of $m(t)$ according to Eqn. (5.6) and hence calculate $m(W)$ and $m(\nu)$ from Eqns. (5.9) and (5.10).

The distributions of the measured $m(t)$ values and $m(t) - m(W)$ mass differences are shown in Figure 14 for a set of 100000 pseudo-experiments. The precision of the top quark mass measurement is ~ 8 GeV, while the uncertainty on the measurement of $m(t) - m(W)$ is ~ 2 GeV. A 95%(68%) upper limit on the neutrino mass of 30(16) GeV is obtained. These
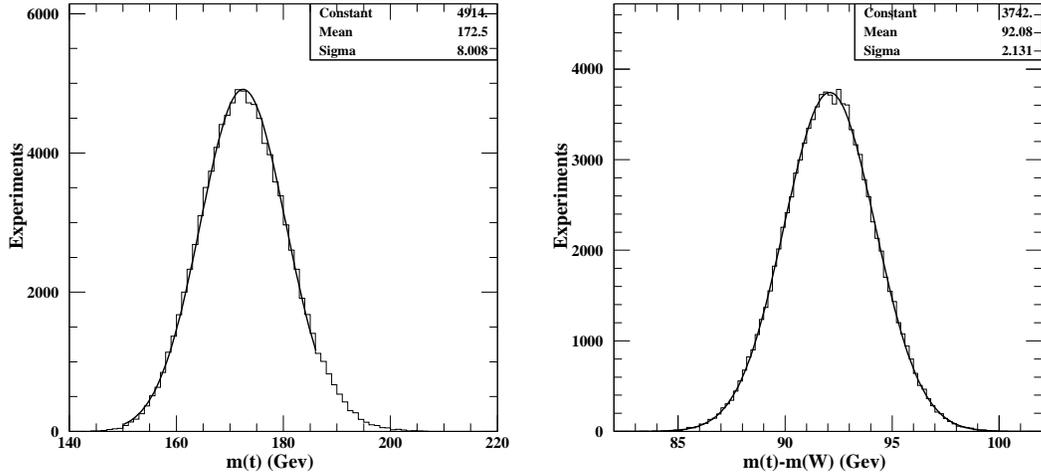
Figure 14: Distributions of the calculated top mass (left) and $m(t) - m(W)$ mass difference for 100k experiments. The assumed statistics is 3 fb^{-1}.

results may appear to be disappointing when compared with the $\sim$1 GeV $m(t)$ precision expected to be obtained at the LHC from semileptonic $t\bar{t}$ events for the same assumptions on b-jet energy scale uncertainty [29]. Here however we have made no assumptions about the masses of the W or neutrino and so 8 GeV is the stand-alone precision with can be obtained with the technique. The end-point measurements used in this technique are primarily sensitive to mass differences and so if the mass of the W were assumed to be known the precision of the measurement of $m(t)$ would improve to $\sim$2 GeV, dominated by the systematics associated with the very crude end-point fitting function used for this study.

5.3 A SUSY example

Having demonstrated the proposed mass measurement technique with $t\bar{t}$ events let us now apply the same technique to a SUSY model generating events with a similar final state. An example of such a SUSY model is an MSSM model with a left-handed slepton doublet lighter than the chargino. In this case events with the decay chain

$$\tilde{q} \to q\tilde{\chi}_1^{\pm} \to q\ell\tilde{\nu} \to q\ell\nu\tilde{\chi}_1^0 \tag{5.13}$$

appearing in both legs of the event can be produced. The invisible sparticle at the end of the chain is in this case the sneutrino, since both of its decay products are undetected. This decay chain maps onto Eqn. (5.1) with $\delta \equiv \tilde{q}$, $\beta \equiv \tilde{\chi}_1^{\pm}$, $\alpha \equiv \tilde{\nu}$, $P \equiv q$ and $Q \equiv \ell$.

The decay (5.13) is however not the only decay yielding the final state of interest, with a quark, a lepton and one or more invisible particles on each leg. We consider the following

decay chains:

$$\tilde{q} \to q\tilde{\chi}_1^\pm \to q\nu\tilde{\ell} \to q\nu\ell\tilde{\chi}_1^0 \tag{5.14}$$

$$\tilde{q} \to q\tilde{\chi}_1^\pm \to q\tilde{\chi}_1^0 W \to q\tilde{\chi}_1^0\ell\nu \tag{5.15}$$

$$\tilde{q} \to q\tilde{\chi}_1^\pm \to q\tilde{\chi}_1^0 W \to q\tilde{\chi}_1^0\ell\nu \tag{5.16}$$

For all of these decays, formulas (5.2)–(5.5) are valid, provided that $m(\alpha)$ in (5.2), (5.4) and (5.5) is replaced by $m_{\min}(\alpha)$, defined as the minimum mass of the "pseudo-particle" composed of all of the invisible particles in the decay. Analytical expressions for $m_{\min}(\alpha)$ in terms of the masses of the particles involved in the decays are given in Appendix B. These can be used in Eqns. (5.2) and (5.5).

The case of Eqn. (5.4) deserves special comment. In this case for decay chains (5.14), (5.15) and (5.16) one invisible particle is upstream of the lepton and one downstream. It is therefore not possible to correct for the upstream momentum, since it is not possible to separate the momentum of the neutrino and of the $\tilde{\chi}_1^0$. However, if one performs the boost correction assuming that all of the observed missing transverse momentum is downstream of the lepton, the distributions for $M_{CT}^{\max}(Q, Q')$ still possess end-points at positions given by Eqn. (5.4) with the $m_{\min}(\alpha)$ values defined in Appendix B.

Based on measurements of the end-point positions k_1, k_2 and k_3, one can calculate the masses of the squark and of the chargino independently from the decay mode of the $\tilde{\chi}_1^\pm$. This is a remarkable achievement, as it shows that it is possible to perform an absolute measurement of the chargino mass through its leptonic decay notwithstanding the fact that two invisible sparticles are present in the decay of each chargino. The interpretation of the meaning of the measured $m(\alpha)$ *is* dependent on the chargino decay mode, and the analysis based on the measurement of k_1, k_2, k_3 and k_4 does not allow the discrimination of the different expressions given in Appendix B.

It should be noted that the mass hierarchy and coupling structure implied by the presence of the decay chain given by Eqn. (5.13) imply also the existence, with a significant branching ratio, of the chain:

$$\tilde{q} \to q\tilde{\chi}_2^0 \to q\ell\tilde{\ell}_L \to q\ell\ell\tilde{\chi}_1^0, \tag{5.17}$$

which can be easily selected by requiring the presence of two leptons with the same flavour and opposite sign. This 'golden channel' for SUSY mass measurement at the LHC can potentially provide additional information regarding the masses of sparticles involved in the chargino decay chain. In the following we shall not show a complete analysis along these lines, which has been already developed in detail in e.g. Refs. [20, 21, 3]. We shall limit ourselves instead to showing for our example model that the invariant mass of two OS-SF leptons does give a characteristic end-point structure from the $\tilde{\chi}_2^0 \to \ell\tilde{\ell}$ decay. Starting from this end-point, and combining it with the hard jets in the events it is possible to measure the masses of $\tilde{q}$, $\tilde{\chi}_2^0$ $\tilde{\ell}$ and $\tilde{\chi}_1^0$ [20, 21, 3]. It is then straightforward to insert the measured values of these masses into Eqns. (5.2)–(5.5) and observe that under the assumption of decays (5.14), (5.15), and (5.16) the mass measurements from the two analyses are inconsistent.

Parameter	Value (GeV)	Parameter	Value (GeV)
$m(\tilde{g})$	520.0	$m(\tilde{u_L})$	503.4
$m(\tilde{e_L})$	157.1	$m(\tilde{\nu_e})$	135.7
$m(\tilde{\chi}_1^{\pm})$	231.5	$m(\tilde{\chi}_2^0)$	232.0
$m(\tilde{\chi}_1^0)$	117.2		

Table 2: Masses of the relevant sparticles for the example MSSM point.

End-point	Position: Chain (5.13)	Position: Chain (5.14)
$m^{\max}(q, \ell)$	362.1	297.7
$M_{CT}^{\max}(q, q')$	396.9	396.9
$M_{CT}^{\max}(\ell, \ell')$	151.9	69.7
$M_{CT}^{\max}([q\ell][q'\ell'])$	727.2	668.5

Table 3: Expected end-point positions in GeV for the decay chains (5.13) and (5.14).

In order to explore the feasibility of this measurement technique, we used `HERWIG` `6.5` [33, 34] to generate events from a toy MSSM model incorporating the mass hierarchy present in decay chain (5.13). The masses of all of the squarks were set to 500 GeV and those of all the sleptons to 150 GeV. The three gaugino masses M_1, M_2 and M_3 were set respectively to 120, 250 and 520 GeV while the higgsino mass parameter μ was set to 400 GeV, $\tan\beta$ to 10, and m_A to 400 GeV. The trilinear couplings were set to zero. The relevant sparticle masses, as calculated by `ISASUSY` `7.75` [35] are listed in Table 2. The expected end-point positions for the chains (5.13) and (5.14) are listed in Table 3, using the results of the discussion above regarding the treatment of $m(\alpha)$ in decay chain (5.14).

A total of 800 K events were generated, corresponding to an integrated luminosity of $\sim$12 fb^{-1}. The generated events were passed through the same parameterised detector simulation as for the top sample described in Section 5.2. Events were selected with the following requirements:

1. $N_{\text{jet}} \geq 2$, with $p_T(j_1) > 100$ GeV and $p_T(j_2) > 50$ GeV.

2. $E_T^{miss} > 100$ GeV.

3. $N_{\text{lep}} = 2$, where lep = e/μ(isolated) and $p_T(l_2) > 20$ GeV. The two leptons were required to possess different flavours.

4. Veto all events with jets with $p_T(j_1) > 20$ GeV labelled as a b-jet or τ-jet.

The veto on b and τ labelled jets was applied to reduce the SUSY background from events containing top quark or τ lepton decays.

The requirement of leptons with different flavour reduces the signal by a factor two, but it is necessary, as the same-flavour signal is dominated by SUSY background events in which the two leptons are produced in the decay chain (5.17). This is demonstrated in Figure 15 which shows the lepton-lepton invariant mass distribution for opposite-sign same-flavour

lepton pairs. The full line is the inclusive distribution, and exhibits the characteristic end-point structure from decay (5.17) [20]; the grey (red) area indicates lepton pairs from the decays (5.13) and (5.14). Figure 15 demonstrates also that the characteristic lepton-lepton invariant mass end-point from the $\tilde{\chi}_2^0 \rightarrow \ell\tilde{\ell}$ decay chain is indeed observable for this model.

Following application of the selection cuts described above the only significant remaining background was from $t\bar{t}$ production and only this background is considered in the following. Approximately 9700 SUSY events passed cuts 1–4. Of these 7200 were indeed events in which both the muon and the electron were produced directly in the decay of a sparticle from the chains (5.13) or (5.14). In the remaining events at least one of the leptons was generated by the decay of a tau lepton produced in one of the two legs of the event. The number of $t\bar{t}$ background events was approximately 1400.

The parton-level distributions for the observables $m(q^{(\prime)}, \ell^{(\prime)})$, $M_{CT}([q\ell], [q'\ell'])$, $M_{CT}(q, q')$ and $M_{CT}(\ell, \ell')$ are shown in Figure 16 for all events passing the selection cuts in which both legs in the event contain the chain (5.13) or the chain (5.14). The contransverse mass observables have been corrected for transverse boosts according to the procedure described in Section 2.2. For the reasons discussed in Section 5.2 we shall not measure or exploit the $M_{CT}([q\ell], [q'\ell'])$ end-points in the following analysis, nor the non-boost-corrected $M_{CT}(b, b')$ and $M_{CT}(\ell, \ell')$ versus p_b end-points. Nevertheless such constraints could be useful for validating mass measurements obtained from the other observables.

The first step in the detector-level analysis is the calculation of the invariant mass
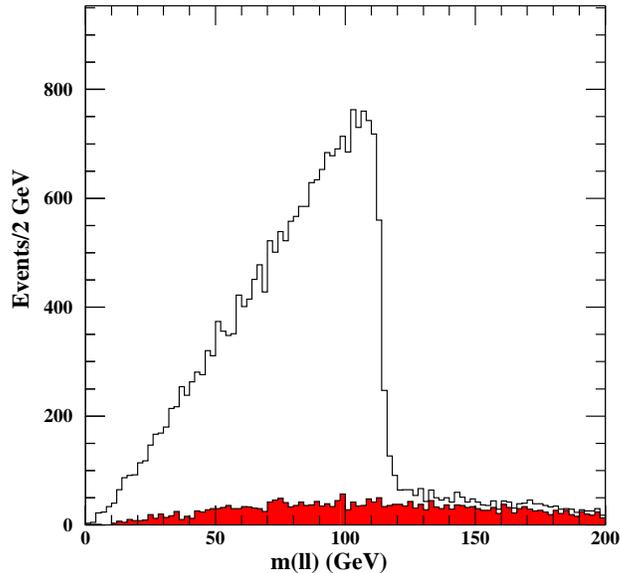
Figure 15: Detector-level lepton-lepton invariant mass for opposite-sign same-flavour lepton pairs after the selection cuts except with the requirement of different flavours for the leptons. The full line is the inclusive distribution while the grey (red) area indicates the distribution for lepton pairs from the decays (5.13) and (5.17).
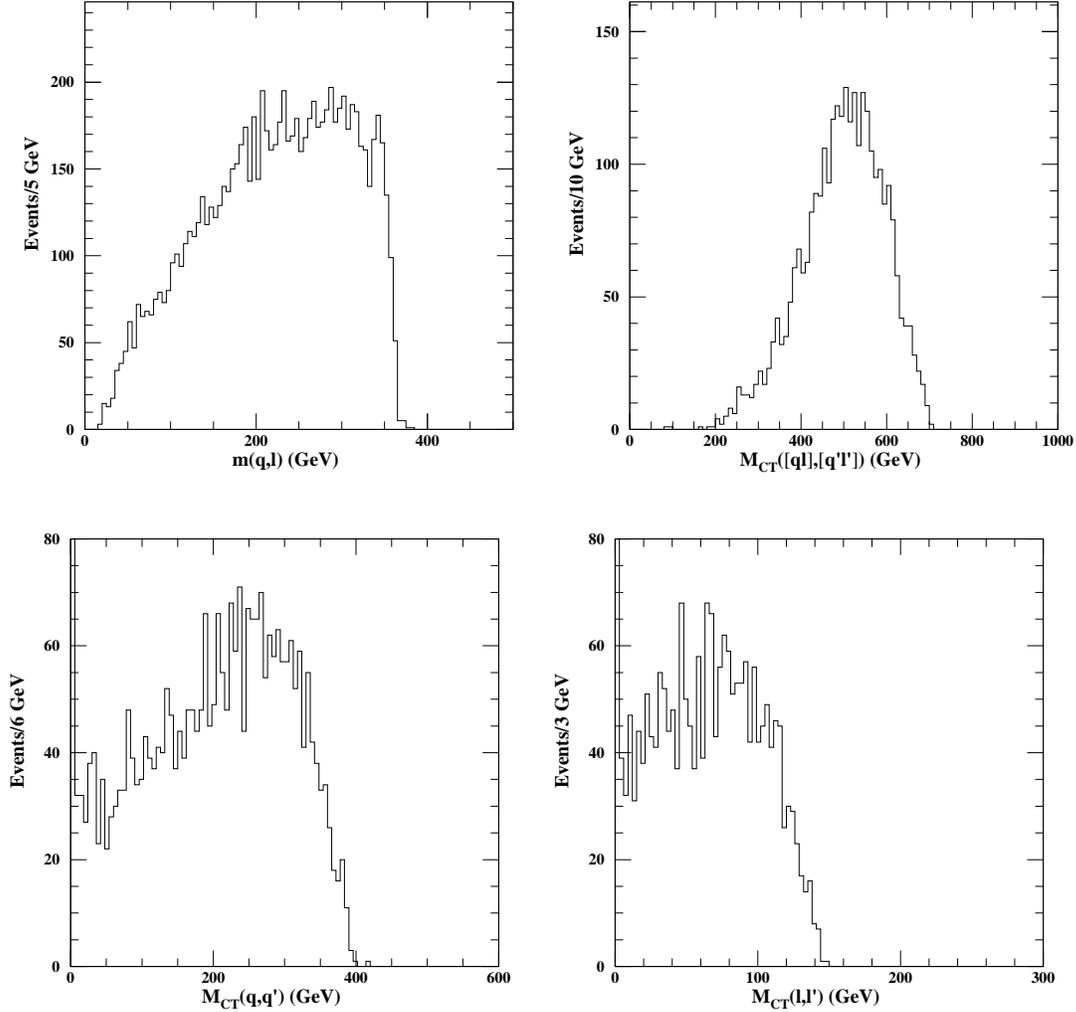
Figure 16: Parton-level distributions of $m(q^{(\prime)}, \ell^{(\prime)})$ (top-left), $M_{CT}([q\ell], [q'\ell'])$ (top-right), $M_{CT}(q, q')$ (bottom-left) and $M_{CT}(\ell, \ell')$ (bottom-right) for SUSY events passing the selection cuts where both leptons are generated by decay chain (5.13).

of each lepton with each of the two leading jets in the event. The distribution of the minimum of these two masses for each lepton is plotted in Figure 17 and displays an end-point at around 360 GeV, as expected from chain (5.13). The detector-level distributions of $M_{CT}(q, q')$ and $M_{CT}(\ell, \ell')$ are plotted in Figure 18 and also display end-points at the positions expected for chain (5.13). Only the distribution of $M_{CT}(\ell, \ell')$ values for events with $A_{x(\text{lab})} < 0$ is shown. This is due to the fact that the distribution at truth level for $A_{x(\text{lab})} < 0$ hits the nominal end-point, whereas that for $A_{x(\text{lab})} > 0$ runs out of statistics approximately 10 GeV below the nominal position (see Figure 19(left)), leading to a biased fitted end-point position at detector level (see Figure 19(right)). This arises because only a very small boost correction (with $E_{\delta\delta}^{\text{est}} = E_{cm}$) can be applied in the $A_{x(\text{lab})} > 0$ case and hence the resulting corrected M_{CT} value is more conservative than in the $A_{x(\text{lab})} < 0$
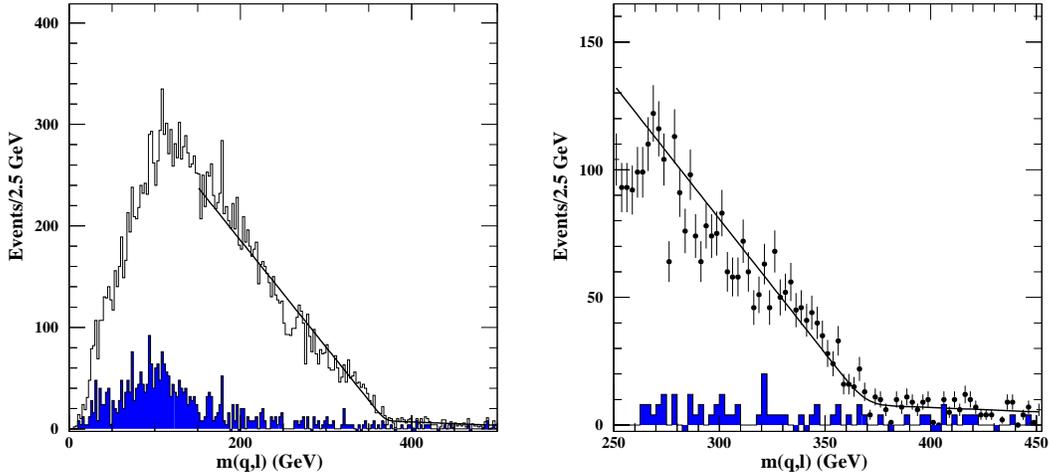
Figure 17: Detector-level distribution of the minimum value of $m(q^{(\prime)}, \ell^{(\prime)})$ for SUSY events passing the selection cuts. The dark grey (blue) histogram indicates the $t\bar{t}$ background. The complete distribution is shown on the left while the region near the end-point is expanded on the right. The fit to the end-point function given in Eqn. (5.12) is shown.

End-point	Truth (GeV)	Measured (GeV)
$m^{\max}(q, \ell)$	362.1	$369.2 \pm 2 \pm 5 \pm 1.5$
$M_{CT}^{\max}(q, q')$	396.9	$401.7 \pm 4.8 \pm 5 \pm 4$
$M_{CT}^{\max}(\ell, \ell')$ $(A_x < 0)$	151.9	$149.3 \pm 1.5 \pm 3 \pm 0.8$

Table 4: End-point positions in GeV. The first uncertainty is statistical, while the second and third are respectively the uncorrelated systematic and correlated energy scale uncertainties. The expected end-point positions from Eqns. (5.2), (5.3) and (5.4) are listed in the column labelled 'Truth'. The assumed integrated luminosity is 12 fb^{-1}

case. This effect is most evident when considering $M_{CT}(\ell, \ell')$ because of the potentially large boosts generated by the recoiling bb' system. The same effect, although numerically less evident, is present also in the top quark analysis but is masked by the smearing of the end-point due to the W natural width. We choose here to use the larger of the two fitted end-point positions, which must be nearer to the true value.

In order to explore the approximate potential precision of mass measurements obtained with this technique, we fit the end-points of the distributions with the smeared linear function given in Eqn. (5.12). The caveats associated with this technique discussed in Section 5.2 are also relevant here. In the case of the $M_{CT}(\ell, \ell')$ distribution we only fit the distribution of events with $A_{x(\text{lab})} < 0$, as discussed above. The fitted distributions are shown in Figures 17 and 18. The results of the end-point fits are listed in Table 4, where the first uncertainty is the statistical uncertainty from the MINUIT [30] fitting program for the chosen fit interval, the second is the systematic uncertainty obtained by varying the fit interval and the third uncertainty is the correlated systematic uncertainty derived
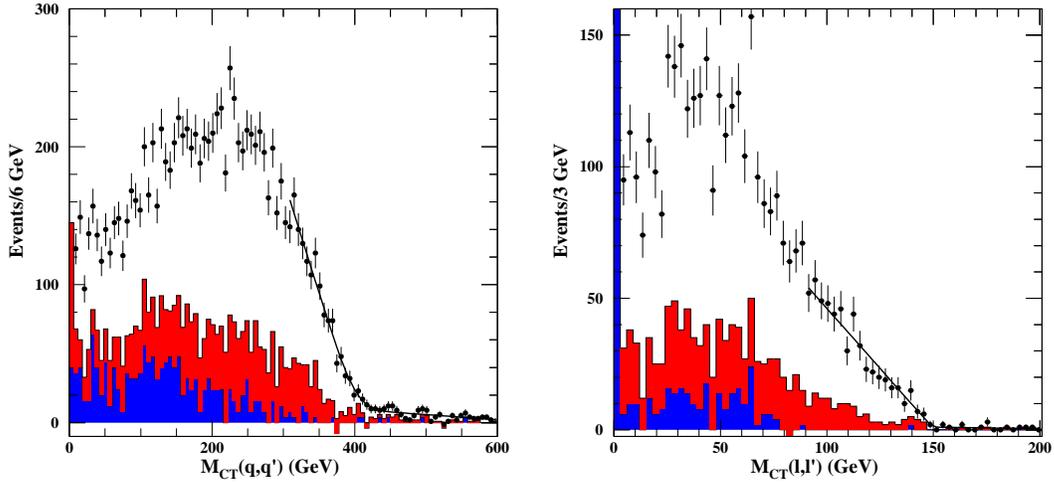
Figure 18: Detector-level distributions of $M_{CT}(q, q')$ (left) and $M_{CT}(\ell, \ell')$ with $A_{x(\text{lab})} < 0$ (right) for SUSY events passing the selection cuts. The light grey (red) histogram is the distribution of events in which at least one of the two leptons was not produced directly from the decay of a sparticle. The dark grey (blue) area indicates the $t\bar{t}$ background. The fits to the end-point function given in Eqn. (5.12) are shown.
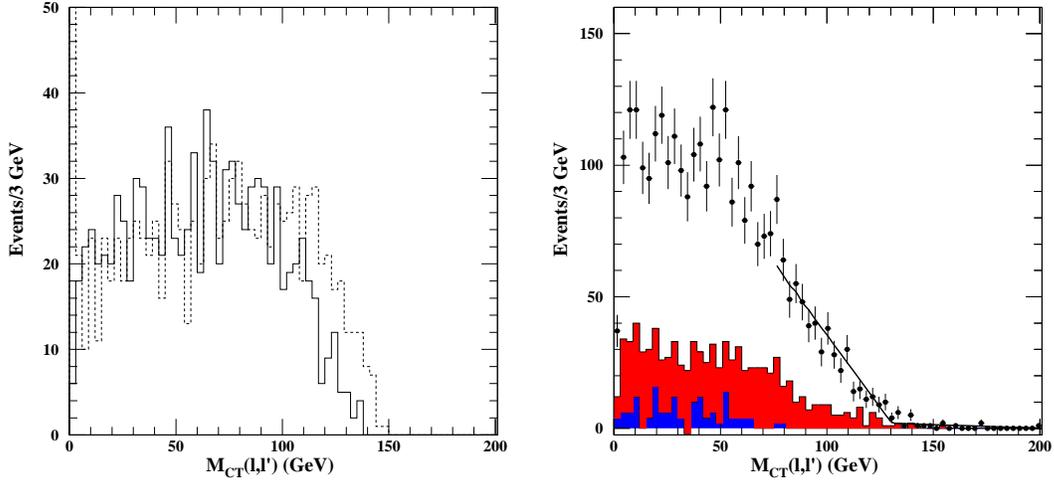
Figure 19: Distributions of $M_{CT}(\ell, \ell')$ at parton-level (left) and at detector-level (right) for SUSY events passing the selection cuts. In the left-hand figure the dashed histogram is the distribution of events with $A_{x(\text{lab})} < 0$ while the full histogram is that of events with $A_{x(\text{lab})} > 0$. In the right-hand figure all events possess $A_{x(\text{lab})} > 0$ and the shaded histograms and fitted curve are as for Figure 18. The fitted end-point position is 133.6 GeV.

from assumed energy scale uncertainties of 1% for jets and 0.1% for leptons [31]. As for the top study the quoted uncertainties should be considered approximate and could be improved with the use of better end-point fitting functions, for instance templates derived

from Monte Carlo simulation studies.

If we use the measured end-point positions to calculate the masses of the sparticles using Eqns. (5.6), (5.3) and (5.4) we obtain an uncertainty of 20 GeV on the absolute squark mass, an uncertainty of 6 GeV on the difference between the squark mass and the masses of the other sparticles, and an uncertainty of 3 GeV on the chargino-sneutrino mass difference. We have thus shown with a toy SUSY model that it is possible to achieve a stand-alone measurement of sparticle masses using the contransverse mass technique applied to events containing two symmetric sequential two-step two-body decay chains.

6. Conclusions

In this paper we have extended the contransverse mass technique for measuring the masses of pair-produced semi-invisibly decaying heavy particles so that it can be applied to events with non-negligible boosts of the CoM frame of the heavy states in the laboratory transverse plane. We have demonstrated the modified technique with case studies measuring the masses of the top quark, W and neutrino in fully leptonic $t\bar{t}$ events, and the masses of sparticles in SUSY events with a similar final state. The case studies presented here are in many respects more detailed than previous studies of alternative strategies and illustrate well the potential utility of the contransverse mass technique.

Acknowledgements

Note added to version 2: Since version 1 of this paper was released onto arXiv a paper [38] has been released which also derives Eqn. (4.9). The boost-dependence study described in Section 4.2, which appeared in version 2 of this paper, was carried out without knowledge of Ref. [38], however we are happy to acknowledge that Eqn. (4.9) appeared in Ref. [38] first.

A. The connection between $M_{T2}(\chi)$ and M_{CT}

Eqn. (4.1) can be used to study the links between $M_{T2}(\chi)$ [1] and M_{CT}, as we shall now illustrate. In the process we shall obtain an approximate analytical expression for a boost-corrected version of $M_{T2}(\chi)$. The link between the two quantities in the absence of co-linear transverse boosts and for massless visible states was first discussed in Ref. [36].

First, observe that if we assume a value for $m(\alpha)$ and know $M_{CT}^{\max}$ then we can solve Eqn. (4.1) for $m(\delta)$. For any given event we do not know $M_{CT}^{\max}$ however, but rather M_{CT}. Let us therefore substitute M_{CT} for $M_{CT}^{\max}$ to obtain the following solution

$$m_{\rm soln}(\delta) = \left(\chi^2 + A_T + \sqrt{\left[1 + \frac{4\chi^2}{2A_T - m^2(v_1) - m^2(v_2)}\right]\left[A_T^2 - m^2(v_1)m^2(v_2)\right]}\right)^{1/2}, \quad (A1)$$

where $A_T \equiv [M_{CT}^2 - m^2(v_1) - m^2(v_2)]/2$ and χ is the assumed value of $m(\alpha)$. This is identical to the analytical expression for the 'balanced' solution of $M_{T2}(\chi)$ in the absence of co-linear transverse boosts, which was identified in Refs. [37, 7]. In general $m_{\text{soln}}(\delta)$ need not be bounded by $m(\delta)$, because A_T and hence M_{CT} appears in the denominator inside the square-root causing $m_{\text{soln}}(\delta)$ not to be a monotonically increasing function of M_{CT}. Therefore a value of $M_{CT} < M_{CT}^{\max}$ need not generate a value of $m_{\text{soln}}(\delta)$ which is less than the value obtained with $M_{CT} = M_{CT}^{\max}$. Note that if $\chi = 0$ then $m_{\text{soln}}(\delta)$ is nevertheless bounded by $m(\delta)$ because in this special case $m_{\text{soln}}(\delta)$ *is* a monotonically increasing function of M_{CT}.

In general $m_{\text{soln}}(\delta)$ is not invariant under co-linear transverse boosts, because it depends on M_{CT} which is also not invariant. One might consider therefore whether it is possible to correct $m_{\text{soln}}(\delta)$ for such boosts in a similar manner to that used to correct M_{CT} in Section 2.2. The M_{CT} boost-correction procedure minimises M_{CT} with respect to the possible boosts, however this does not necessarily minimise $m_{\text{soln}}(\delta)$ because it is not in general a monotonically increasing function of M_{CT}. Boost-correction can be performed however, as we know not only the minimum possible value of M_{CT} in the $\delta_1 \delta_2$ CoM frame but also the maximum possible value, which is given by the maximum of the M_{CT} values obtained by boosting v_1 and v_2 with respectively $\beta = p_b/E_{\text{cm}}$ and $\beta = p_b/\widehat{E}$ (see Fig. 3). We therefore know the range of CoM frame M_{CT} values which could have occurred in the event.

To proceed we find the turning-points of Eqn. (A1), which lie at the following four values of M_{CT}^2:

$$M_{CT}^2 = \frac{\chi[3m^2(v_i) + m^2(v_j)] \pm 2m(v_i)[m^2(v_i) + m^2(v_j)]}{\chi \pm m(v_i)}, \qquad \text{(A2)}$$

where $i, j = 1, 2$ ($i \neq j$). We then take the minimum of all the $m_{\text{soln}}(\delta)$ values obtained at turning-points where M_{CT} lies within the allowed range identified above. We finally take the minimum of this $m_{\text{soln}}(\delta)$ value and those obtained with M_{CT} set to its extrema. The result is a boost-corrected value of $m_{\text{soln}}(\delta)$.

Now although $m_{\text{soln}}(\delta)$ is not in general bounded by $m(\delta)$ the full analytical expression for $M_{T2}(\chi)$ in the absence of co-linear transverse boosts [37, 7] is so bounded. This is because in those cases where $m_{\text{soln}}(\delta) > m(\delta)$ $M_{T2}(\chi)$ takes on an alternative value corresponding to an 'unbalanced' solution (see e.g. Eqn. (54) in Ref. [37]). The quantities upon which the decision to switch to such an alternative value rests are not themselves boost-invariant. Development of an appropriate boost-correction procedure for these quantities consistent with the parallel boost-correction of $m_{\text{soln}}(\delta)$ requires more work. In the absence of such a correction procedure we can choose to neglect the boost when making this decision, to obtain an approximate analytical form for a boost-corrected version of $M_{T2}(\chi)$.

Note that the quantity calculated here is not the same quantity as the conventional $M_{T2}(\chi)$ used elsewhere, which is boost-independent but currently does not possess a general analytical form. The boost-correction procedure, even if exact (i.e in the absence of the approximation mentioned in the previous paragraph), leads to a quantity which is not in

general equal to the conventional $M_{T2}(\chi)$, although equality is obtained in the absence of co-linear transverse boosts.

The procedure described above for calculating this 'boost-corrected $M_{T2}(\chi)$' quantity is implemented in the boost-correction package described in Section 2.2, available at `http://projects.hepforge.org/mctlib`.

B. Invisible pseudo-particle masses for chargino decay chains

If a heavy sparticle decays via a chain which produces multiple invisible final state particles then the values of $m^{\max}(P,Q)$ and $M_{CT}^{\max}([PQ],[P'Q'])$ can be calculated by constructing an aggregate 'pseudo-particle' α from the invisible particles. The minimum value of $m(\alpha)$, $m_{\min}(\alpha)$, can then be used in end-point formulae, as described in Section 5.3.

If a chargino decays through $\tilde{\chi}_1^\pm \to \tilde{\chi}_1^0 W^\pm \to \tilde{\chi}_1^0 \nu \ell^\pm$ then $\alpha \equiv [\tilde{\chi}_1^0 \nu]$ and $m_{\min}(\alpha)$ is given by:

$$m_{\min}^2(\alpha) = m^2(\tilde{\chi}_1^0) + m(W)\big[E(\tilde{\chi}_1^0) - p\big]\sqrt{\frac{E(W) - p}{E(W) + p}}, \tag{B1}$$

where

$$p \equiv \frac{\sqrt{[m^2(\tilde{\chi}_1^\pm) - m^2(\tilde{\chi}_1^0) - m^2(W)]^2 - 4m^2(\tilde{\chi}_1^0)m^2(W)}}{2m(\tilde{\chi}_1^\pm)}, \tag{B2}$$

$$E(W) = \frac{m^2(\tilde{\chi}_1^\pm) - m^2(\tilde{\chi}_1^0) + m^2(W)}{2m(\tilde{\chi}_1^\pm)}, \tag{B3}$$

$$E(\tilde{\chi}_1^0) = \frac{m^2(\tilde{\chi}_1^\pm) + m^2(\tilde{\chi}_1^0) - m^2(W)}{2m(\tilde{\chi}_1^\pm)}, \tag{B4}$$

and we have assumed $m(\nu) = 0$. If however the chargino decays through $\tilde{\chi}_1^\pm \to \nu \tilde{\ell}^\pm \to \nu \ell^\pm \tilde{\chi}_1^0$, as in decay chain (5.14), then:

$$m_{\min}(\alpha) = \frac{m(\tilde{\chi}_1^\pm)m(\tilde{\chi}_1^0)}{m(\tilde{\ell}^\pm)}, \tag{B5}$$

while if the chargino decays through $\tilde{\chi}_1^\pm \to \ell^\pm \tilde{\nu} \to \ell^\pm \nu \tilde{\chi}_1^0$, as in decay chain (5.13), then $\alpha \equiv \tilde{\nu}$ and $m_{\min}(\alpha)$ is fixed to $m(\alpha)$ given by:

$$m(\alpha) = m(\tilde{\nu}). \tag{B6}$$

Finally, if the chargino decays through the three-body decay $\tilde{\chi}_1^\pm \to \tilde{\chi}_1^0 \ell^\pm \nu$ then $\alpha \equiv [\tilde{\chi}_1^0 \nu]$ and $m_{\min}(\alpha)$ is given by:

$$m_{\min}(\alpha) = m(\tilde{\chi}_1^0). \tag{B7}$$

References

[1] C. G. Lester and D. J. Summers, Phys. Lett. B **463** (1999) 99 [arXiv:hep-ph/9906349].

[2] A. Barr, C. Lester and P. Stephens, J. Phys. G **29** (2003) 2343 [arXiv:hep-ph/0304226].

[3] B.K. Gjelsten, J. Hisano, K. Kawagoe, E. Lytken, D. Miller, M. M. Nojiri, P. Osland and G. Polesello in G. Weiglein *et al.* [LHC/LC Study Group], Phys. Rept. **426** (2006) 47 [arXiv:hep-ph/0410364].

[4] W. S. Cho, K. Choi, Y. G. Kim and C. B. Park, Phys. Rev. Lett. **100** (2008) 171801 [arXiv:0709.0288 [hep-ph]].

[5] B. Gripaios, JHEP **0802** (2008) 053 [arXiv:0709.2740 [hep-ph]].

[6] A. J. Barr, B. Gripaios and C. G. Lester, JHEP **0802** (2008) 014 [arXiv:0711.4008 [hep-ph]].

[7] W. S. Cho, K. Choi, Y. G. Kim and C. B. Park, JHEP **0802** (2008) 035 [arXiv:0711.4526 [hep-ph]].

[8] M. M. Nojiri, Y. Shimizu, S. Okada and K. Kawagoe, JHEP **0806** (2008) 035 [arXiv:0802.2412 [hep-ph]].

[9] D. R. Tovey, JHEP **0804** (2008) 034 [arXiv:0802.2879 [hep-ph]].

[10] A. J. Barr, G. G. Ross and M. Serna, Phys. Rev. D **78** (2008) 056006 [arXiv:0806.3224 [hep-ph]].

[11] M. M. Nojiri, K. Sakurai, Y. Shimizu and M. Takeuchi, JHEP **0810** (2008) 100 [arXiv:0808.1094 [hep-ph]].

[12] W. S. Cho, K. Choi, Y. G. Kim and C. B. Park, Phys. Rev. D **79** (2009) 031701 [arXiv:0810.4853 [hep-ph]].

[13] H. C. Cheng and Z. Han, JHEP **0812** (2008) 063 [arXiv:0810.5178 [hep-ph]].

[14] M. Burns, K. Kong, K. T. Matchev and M. Park, JHEP **0903** (2009) 143 [arXiv:0810.5576 [hep-ph]].

[15] A. J. Barr, A. Pinder and M. Serna, Phys. Rev. D **79** (2009) 074005 [arXiv:0811.2138 [hep-ph]].

[16] K. T. Matchev, F. Moortgat, L. Pape and M. Park, arXiv:0909.4300 [hep-ph].

[17] CDF Collaboration, CDF Note 9679.

[18] W. S. Cho, K. Choi, Y. G. Kim and C. B. Park, Phys. Rev. D **78** (2008) 034019 [arXiv:0804.2185 [hep-ph]].

[19] A. J. Barr, JHEP **0602** (2006) 042 [arXiv:hep-ph/0511115].

[20] H. Bachacou, I. Hinchliffe and F. E. Paige, Phys. Rev. D **62** (2000) 015009 [arXiv:hep-ph/9907518].

[21] B. C. Allanach, C. G. Lester, M. A. Parker and B. R. Webber, JHEP **0009** (2000) 004 [arXiv:hep-ph/0007009].

[22] D. Costanzo and D. R. Tovey, JHEP **0904** (2009) 084 [arXiv:0902.2331 [hep-ph]].

[23] M. Burns, K. T. Matchev and M. Park, JHEP **0905** (2009) 094 [arXiv:0903.4371 [hep-ph]].

[24] K. T. Matchev, F. Moortgat, L. Pape and M. Park, JHEP **0908** (2009) 104 [arXiv:0906.2417 [hep-ph]].

[25] K. Kawagoe, M. M. Nojiri and G. Polesello, Phys. Rev. D **71** (2005) 035008 [arXiv:hep-ph/0410160].

[26] S. Frixione and B. R. Webber, JHEP **0206** (2002) 029 [arXiv:hep-ph/0204244].

[27] S. Frixione, P. Nason and B. R. Webber, JHEP **0308** (2003) 007 [arXiv:hep-ph/0305252].

[28] E. Richter-Was, arXiv:hep-ph/0207355.

[29] The ATLAS Collaboration, "Expected Performance of the ATLAS Experiment, Detector, Trigger and Physics" CERN-OPEN-2008-020 (2008).

[30] F. James and M. Roos, Comput. Phys. Commun. **10** (1975) 343.

[31] ATLAS Collaboration, *ATLAS detector and physics performance Technical Design Report*, CERN/LHCC 99-14/15 (1999).

[32] M. M. Nojiri, G. Polesello and D. R. Tovey, JHEP **0603** (2006) 063 [arXiv:hep-ph/0512204].

[33] G. Corcella *et al.*, JHEP **0101** (2001) 010 [arXiv:hep-ph/0011363].

[34] S. Moretti, K. Odagiri, P. Richardson, M. H. Seymour and B. R. Webber, JHEP **0204** (2002) 028 [arXiv:hep-ph/0204123].

[35] F. E. Paige, S. D. Protopopescu, H. Baer and X. Tata, arXiv:hep-ph/0312045.

[36] M. Serna, JHEP **0806** (2008) 004 [arXiv:0804.3344 [hep-ph]].

[37] C. Lester and A. Barr, JHEP **0712** (2007) 102 [arXiv:0708.1028 [hep-ph]].

[38] K. T. Matchev and M. Park, arXiv:0910.1584 [hep-ph].